Supporting information

Nucleophilic addition reactions of nitrilium derivatives $[B_{12}H_{11}NCCH_3]^-$ and $[B_{12}H_{11}NCCH_2CH_3]^-$. Synthesis and structure of B_{12}-based iminols, amides and amidines.

Julia Laskova, *[a] Ivan Ananiev,[a,b] Irina Kosenko,[a] Alexander Serdyukov,[a,c] Marina Stogniy,[a,c] Igor Sivaev,[a] Mikhail Grin,[c] Andrey Semioshkin[a] and Vladimir I. Bregadze[a]

a. A. N. Nesmeyanov Institute of Organoelement Compounds, Russian Academy of Sciences, 28 Vavilov Str., 119991, Moscow, Russia.

b. G.V.Plekhanov Russian University of Economics, 117997, 36, Stremyanny line, Moscow, Russia.

c. M. V. Lomonosov Institute of Fine Chemical Technology, MIREA - Russian Technological University, 86 Vernadsky Av., 119571, Moscow, Russia.

I NMR and IR spectra

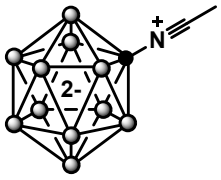

[1]NHEt$_3$

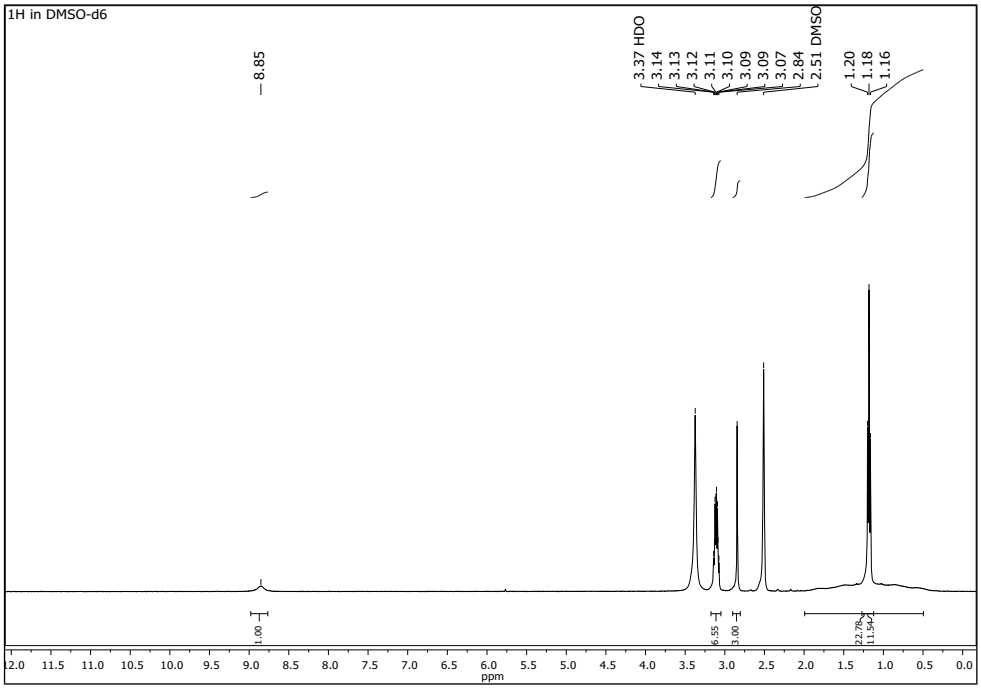

^{1}H-NMR spectrum of [**1**]NHEt$_3$ in DMSO-d$_6$

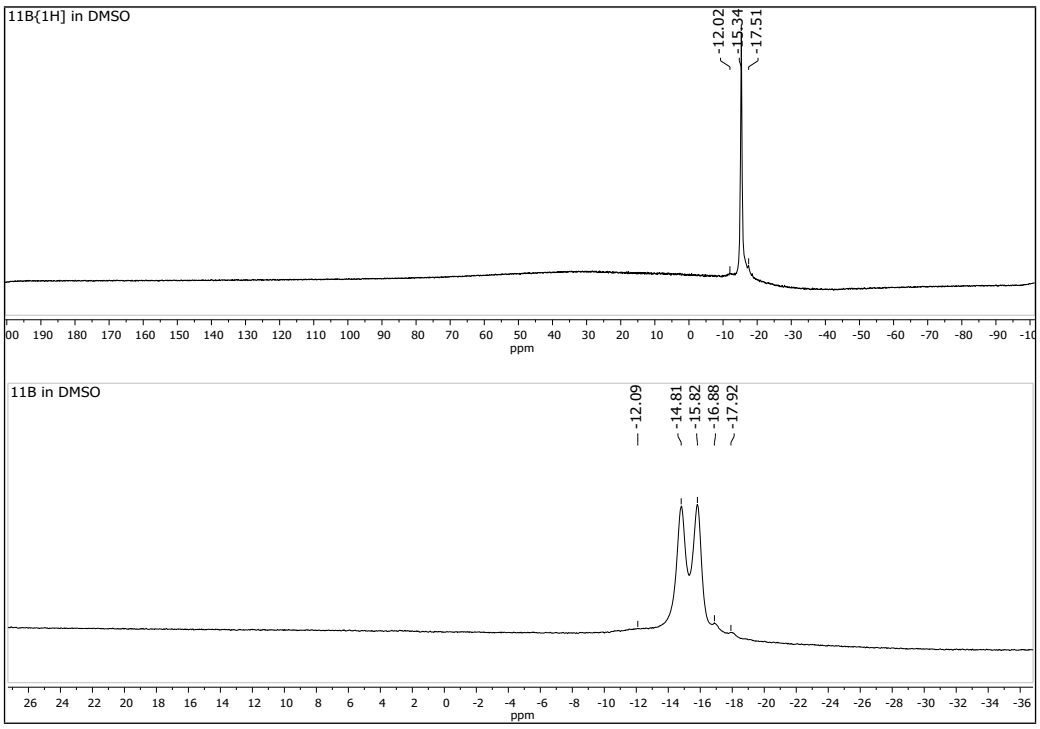

$^{11}B\{^{1}H\}$- and ^{11}B - NMR spectra of [**1**]$NHEt_3$ in DMSO-d_6

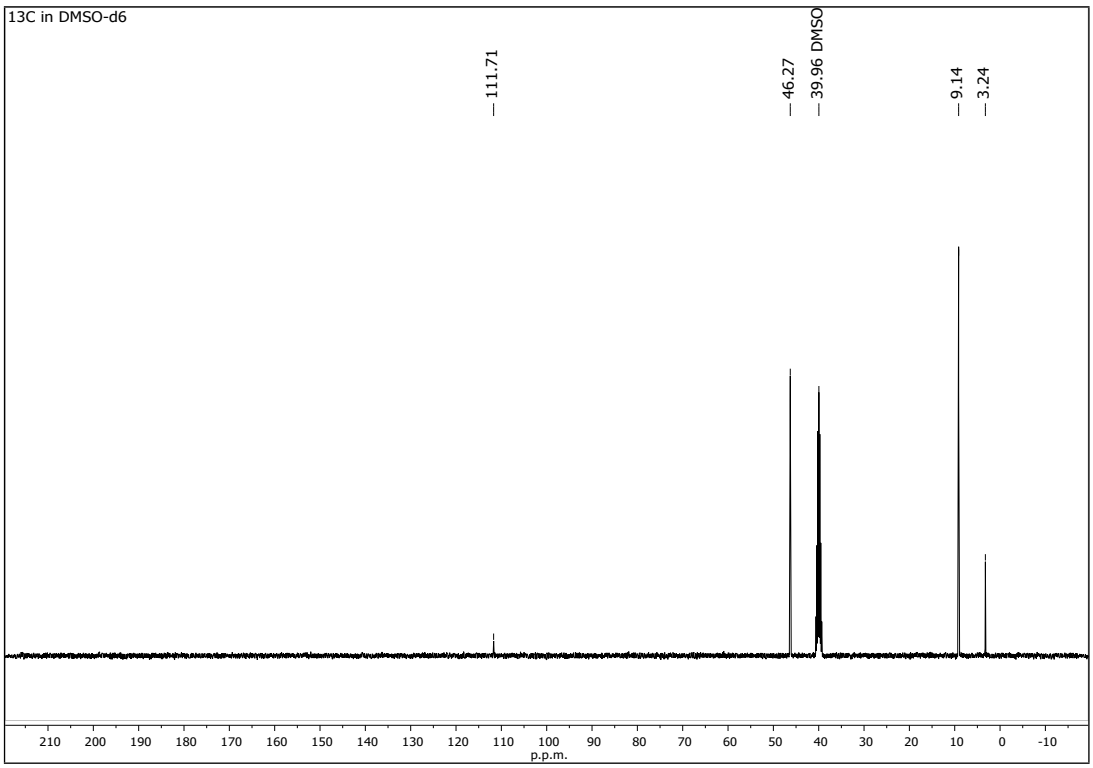

^{13}C - NMR spectrum of [**1**]$NHEt_3$ in DMSO-d_6

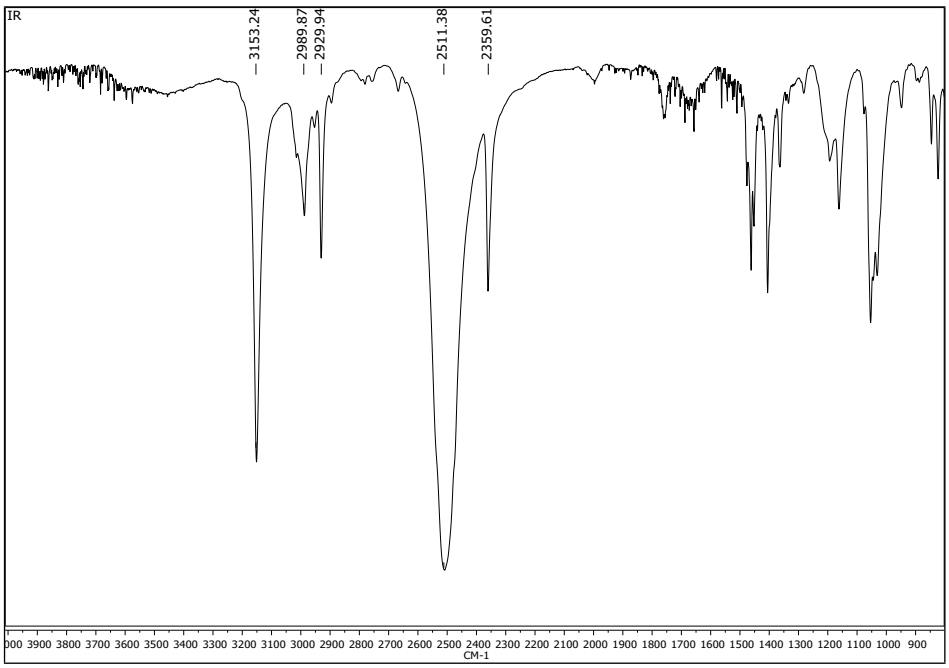

IR - spectrum of [**1**]$NHEt_3$ in KBr

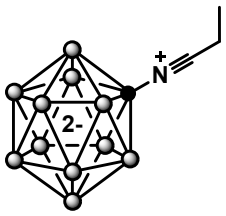

[2]$NHEt_3$

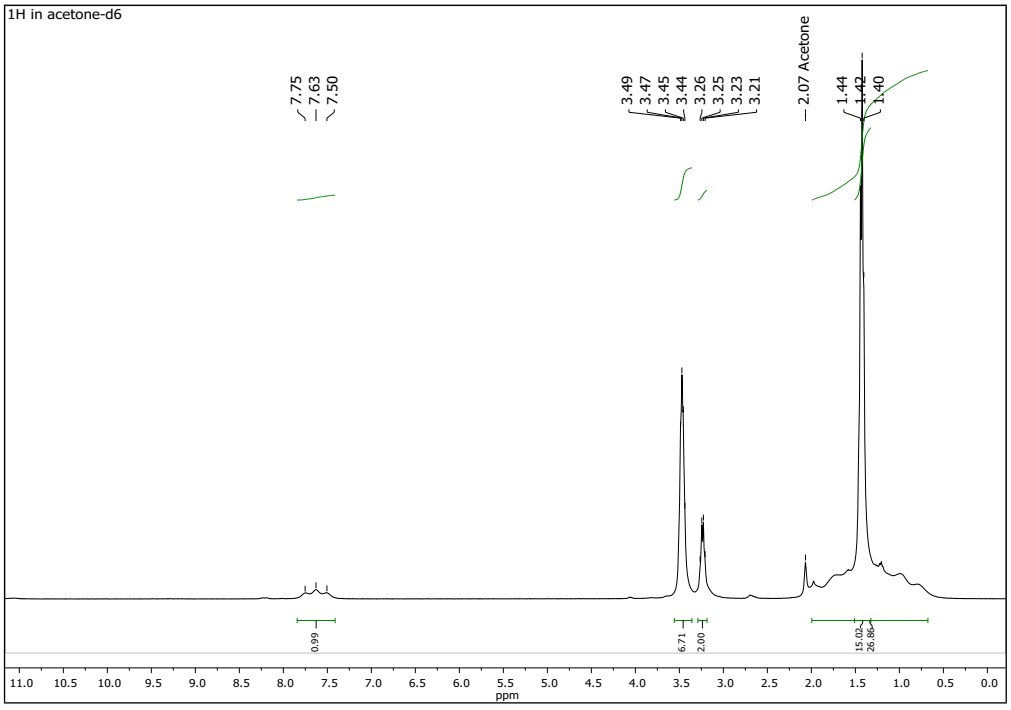

^{1}H-NMR spectrum of [**2**]$NHEt_3$ in acetone-d_6

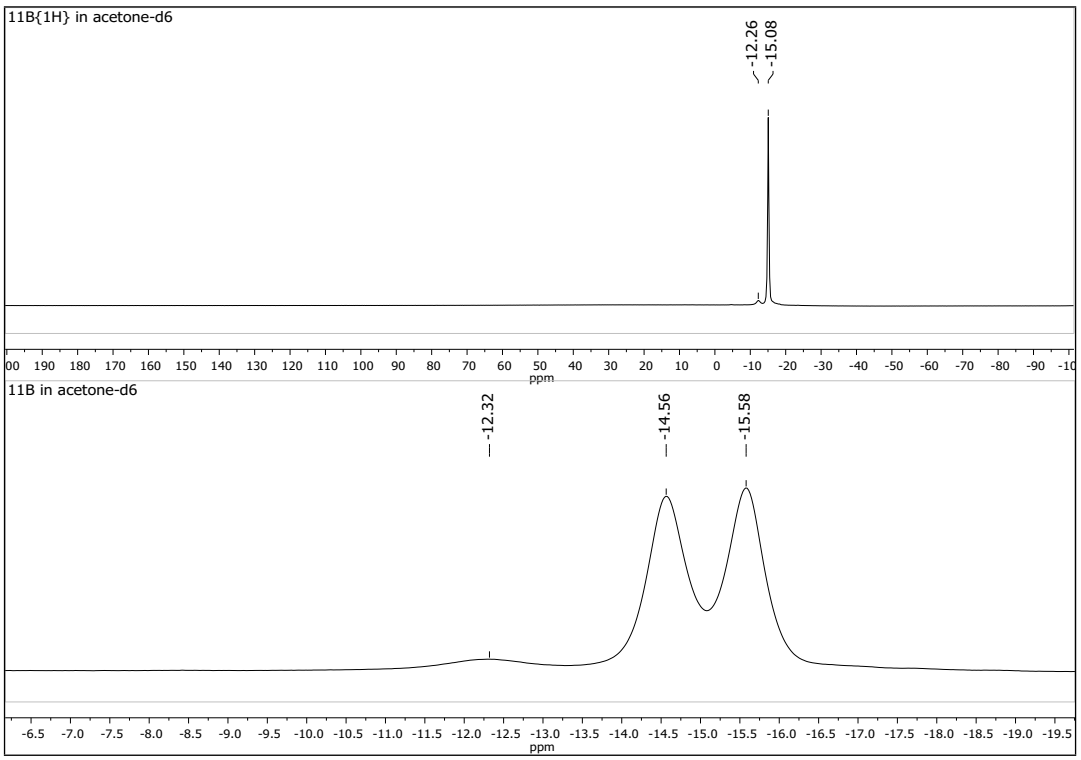

$^{11}B\{^{1}H\}$- and ^{11}B - NMR spectra of [**2**]$NHEt_3$ in acetone-d_6

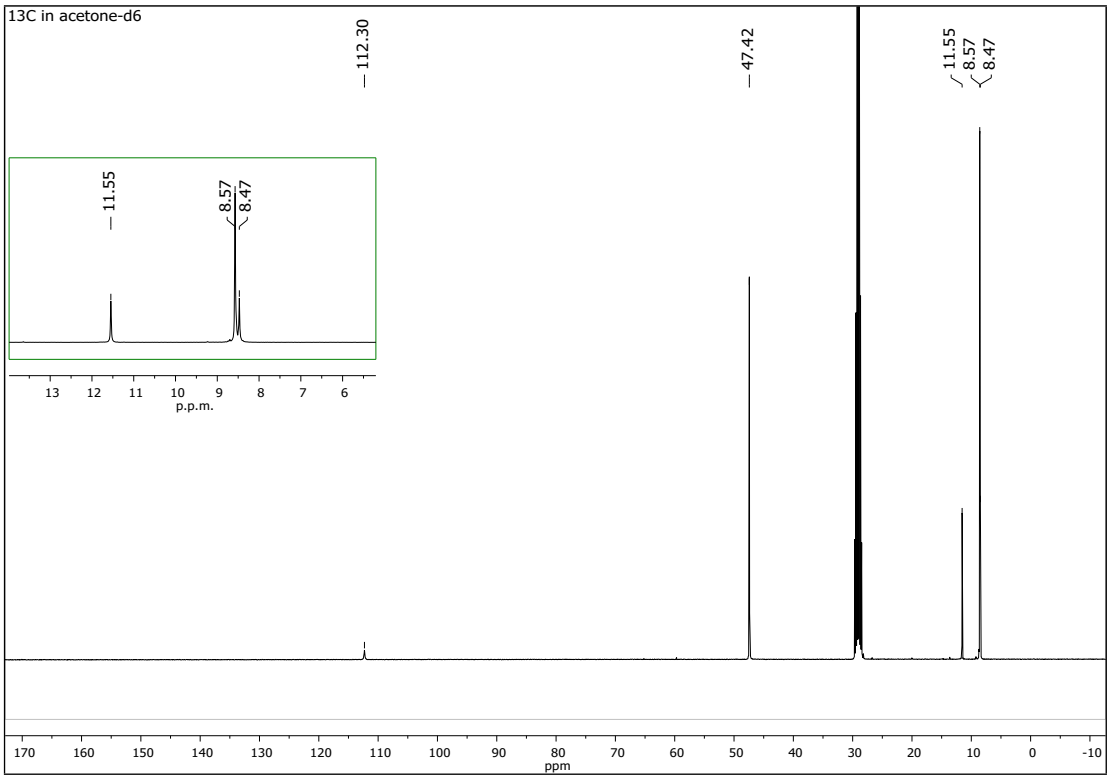

^{13}C - NMR spectrum of [**2**] $NHEt_3$ in acetone-d_6

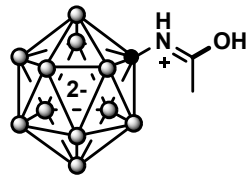

[3]NHEt$_3$

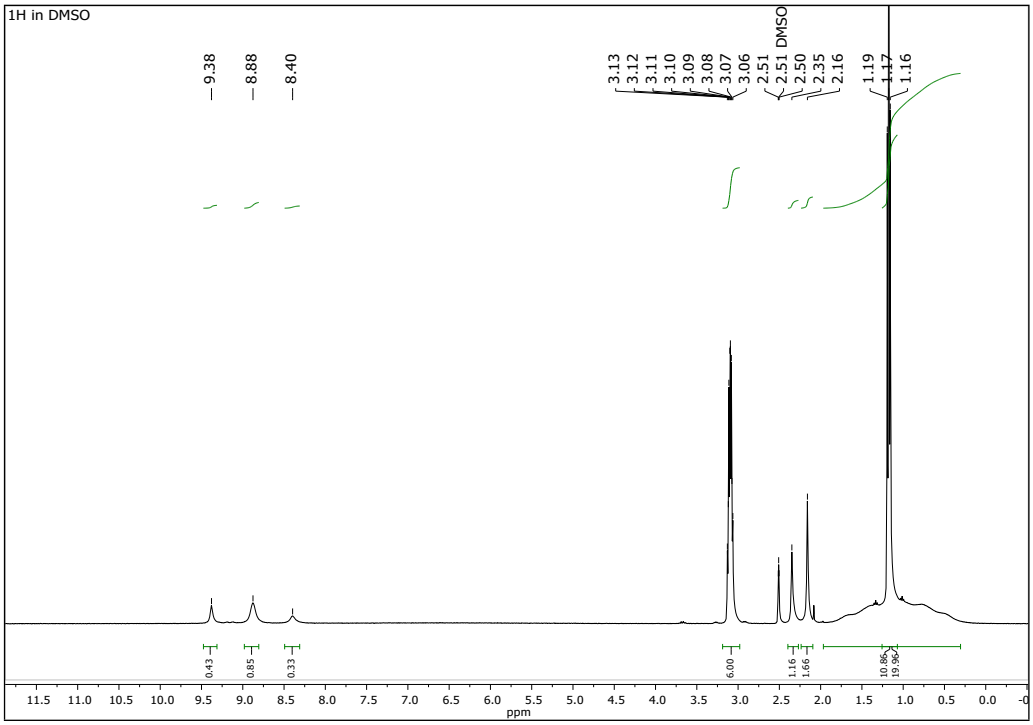

^{1}H-NMR spectrum of [**3**]NHEt$_3$ in DMSO-d$_6$

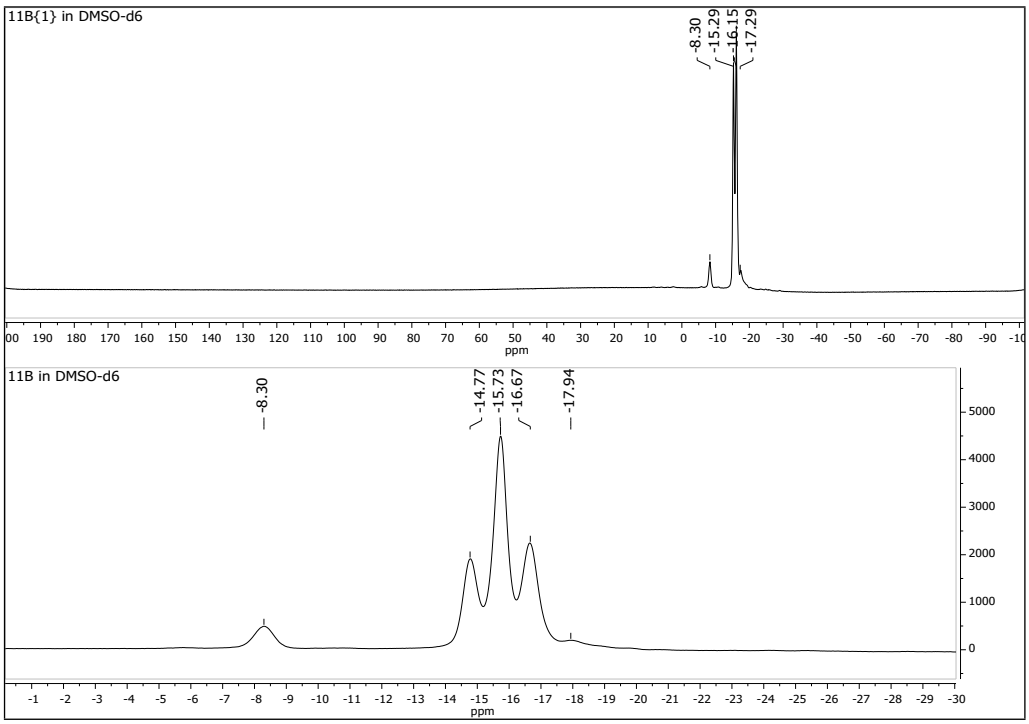

^{11}B{^{1}H}- and ^{11}B - NMR spectra of [**3**]NHEt$_3$ in DMSO-d$_6$

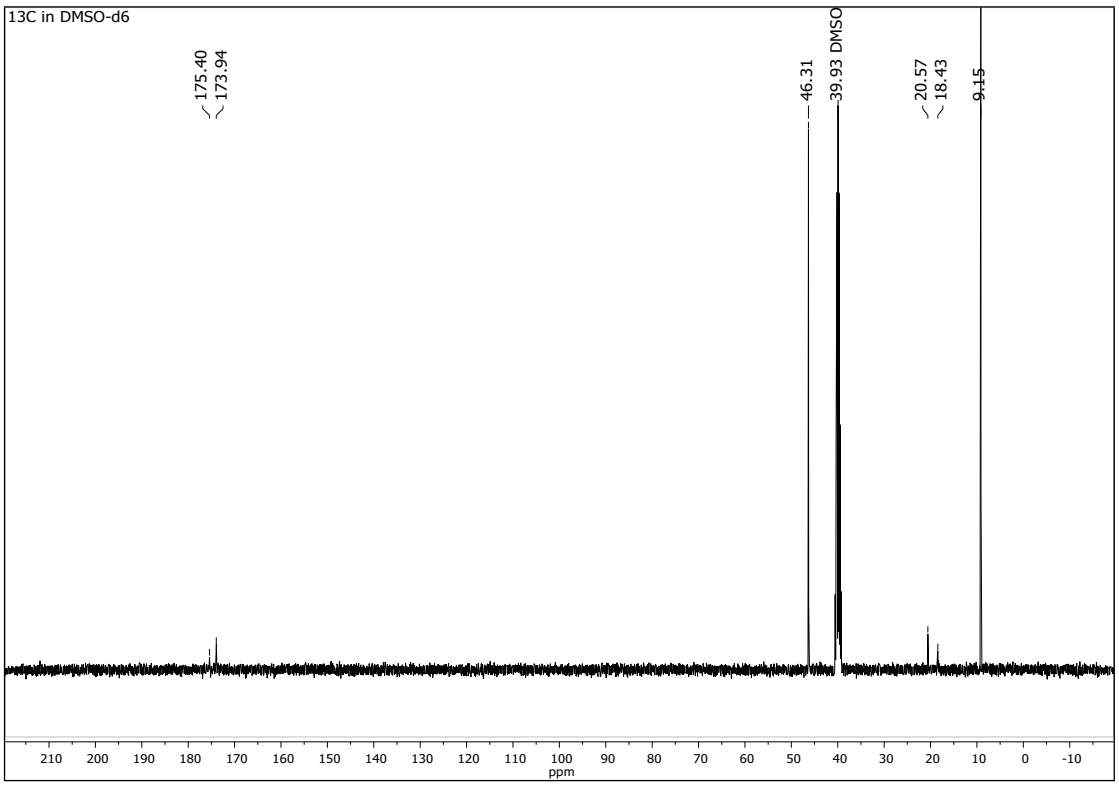

^{13}C - NMR spectrum of [**3**] $NHEt_3$ in DMSO-d_6

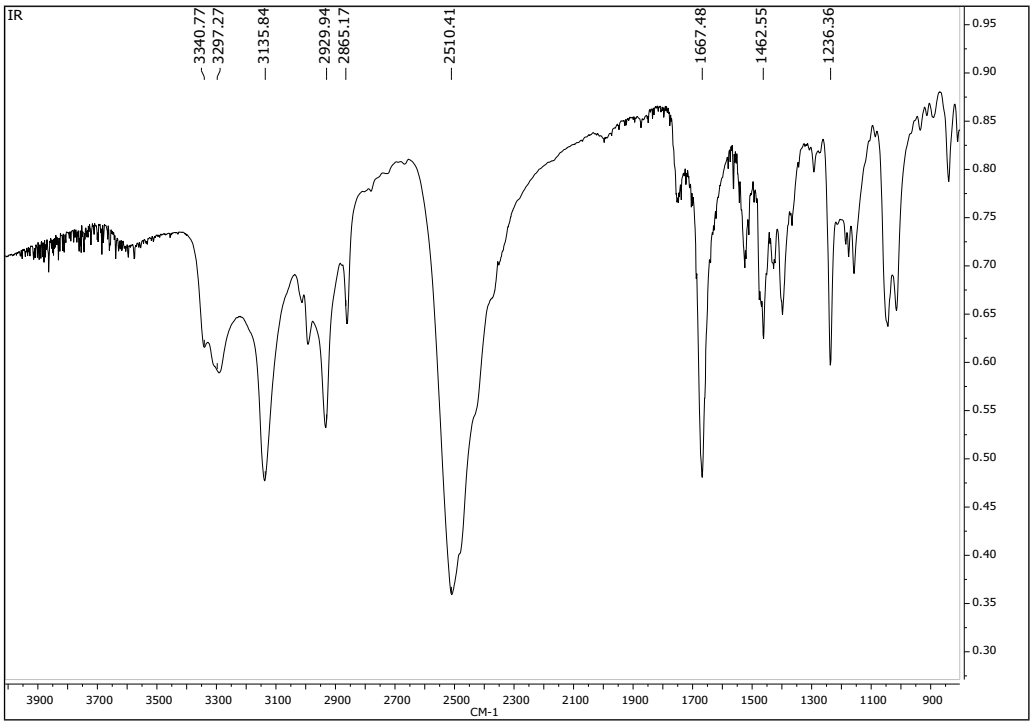

IR - spectrum of [**3**]$NHEt_3$ in KBr

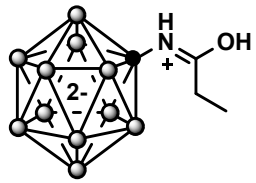

[4]NHEt$_3$

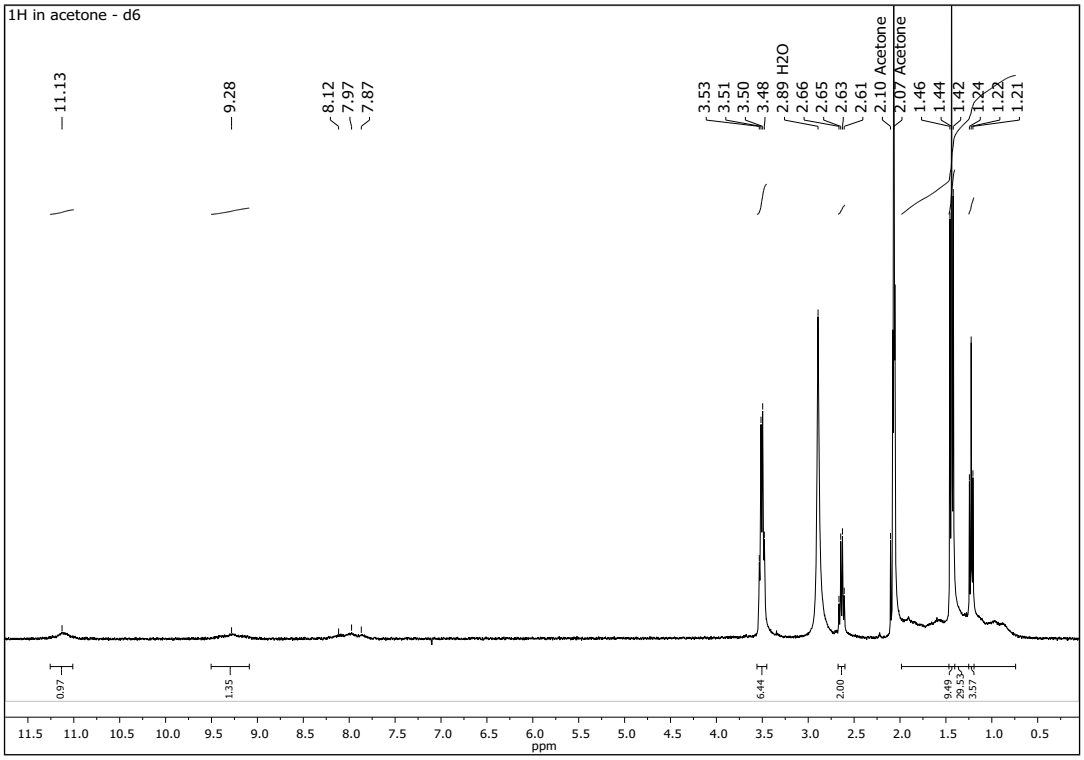

^{1}H-NMR spectrum of [**4**]NHEt$_3$ in acetone-d$_6$

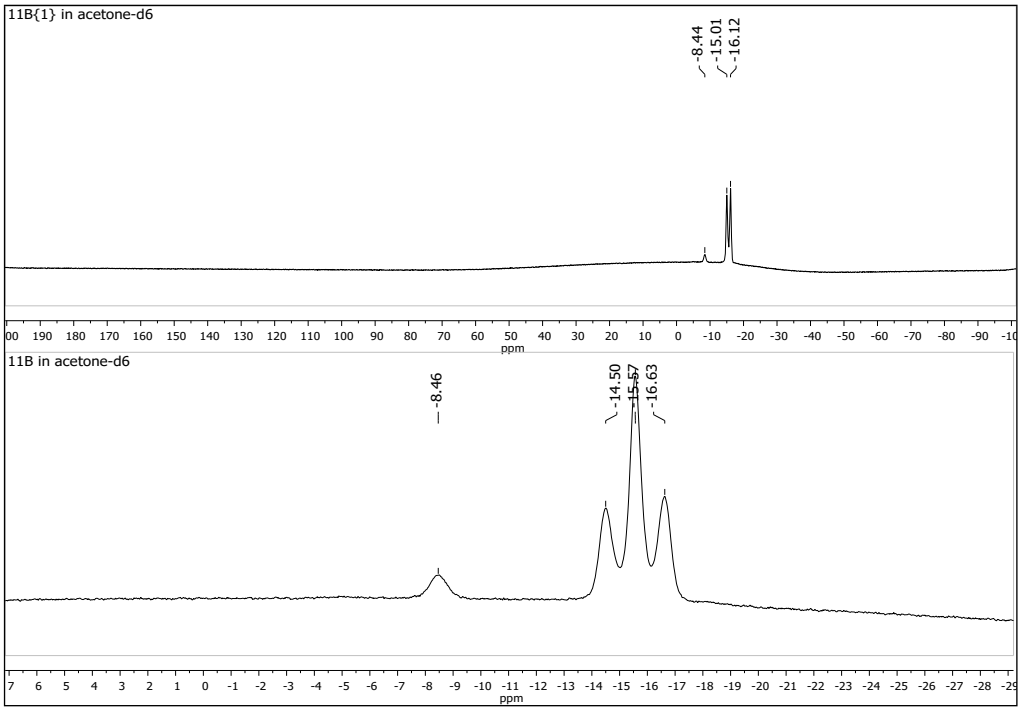

^{11}B{^{1}H}- and ^{11}B - NMR spectra of [**4**]NHEt$_3$ in acetone-d$_6$

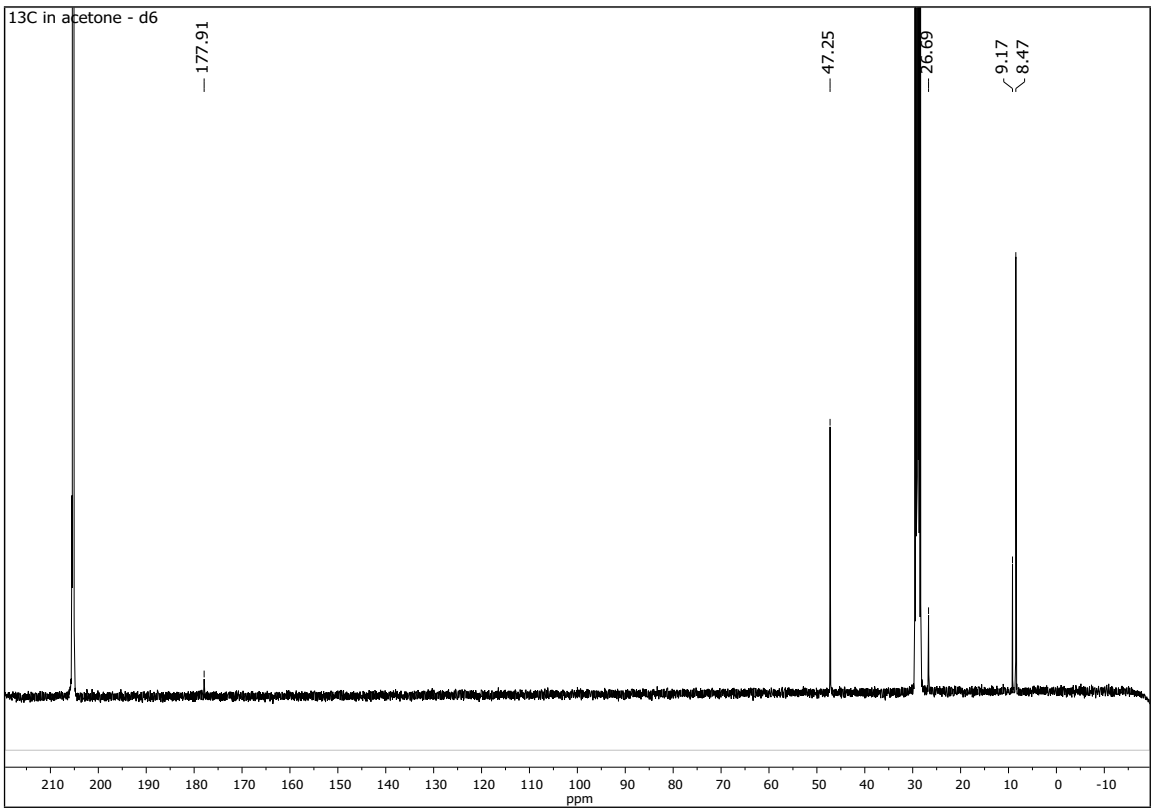

^{13}C - NMR spectrum of [**4**] $NHEt_3$ in acetone-d_6

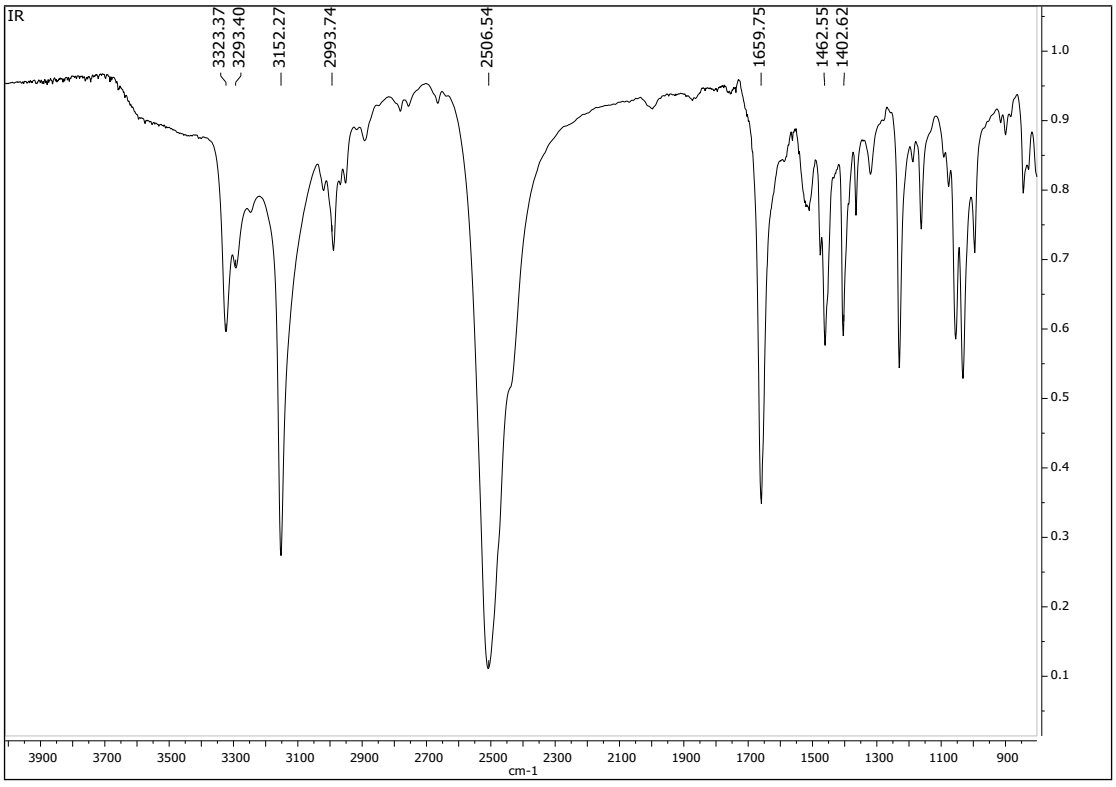

IR - spectrum of [**4**]$NHEt_3$ in KBr

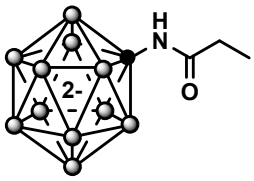

[6](NHEt$_3$)$_2$

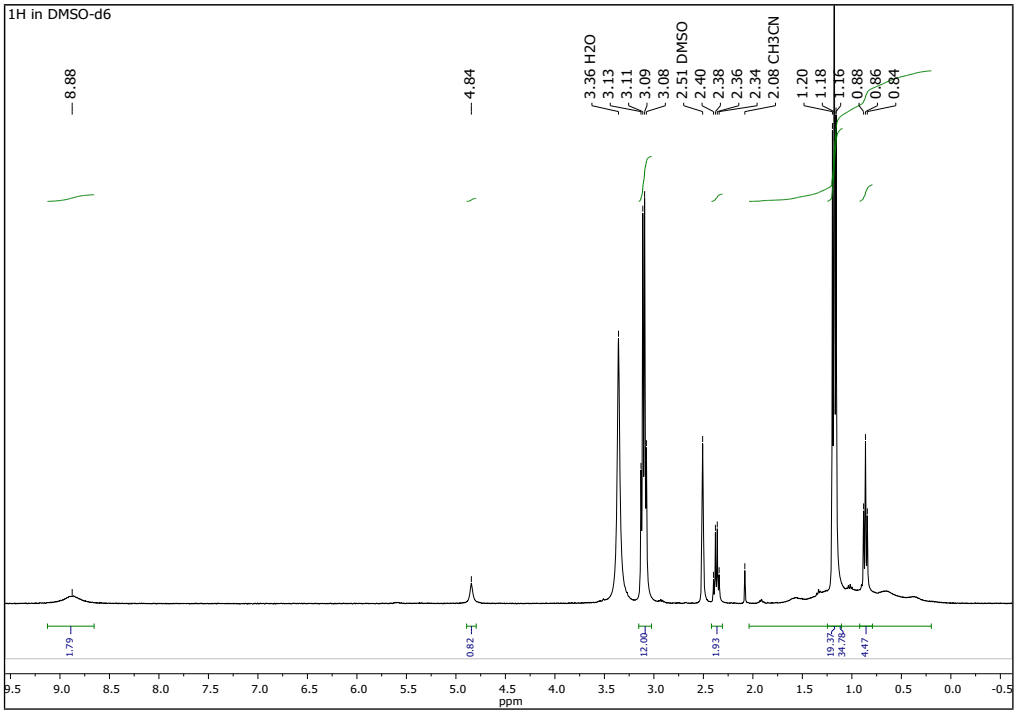

^{1}H - NMR spectrum of [**6**](NHEt$_3$)$_2$ in DMSO-d$_6$

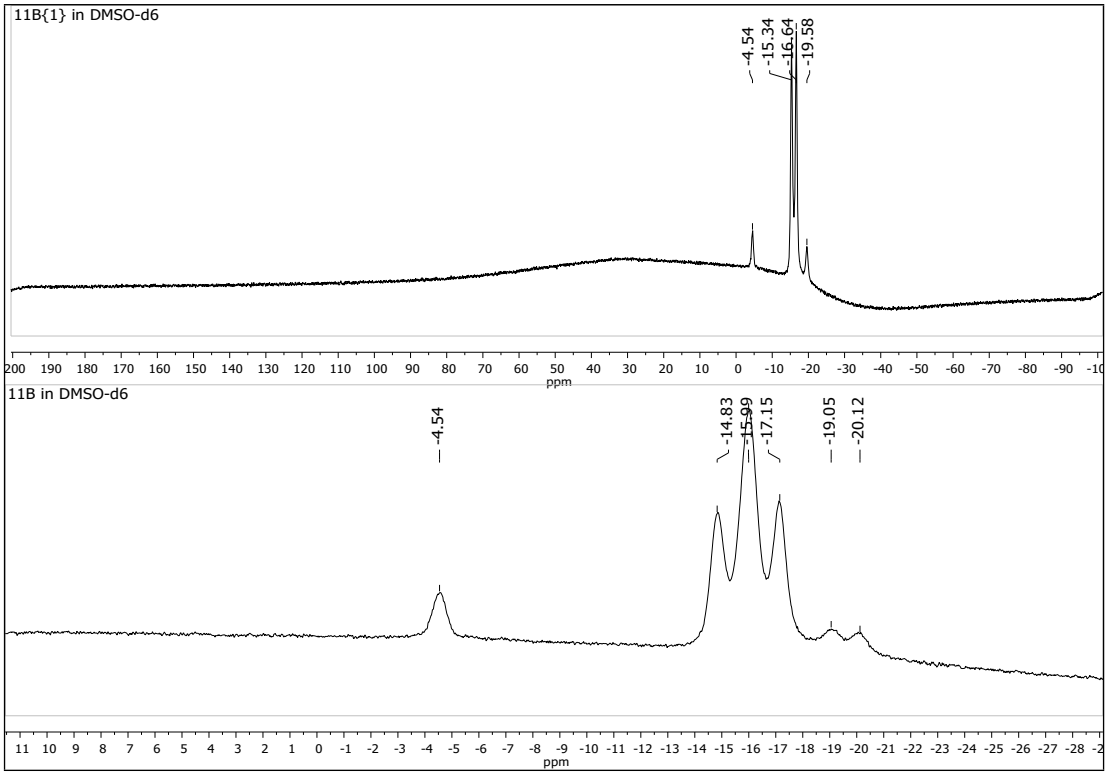

$^{11}B\{^{1}H\}$- and ^{11}B - NMR spectra of [**6**]$(NHEt_3)_2$ in DMSO-d_6

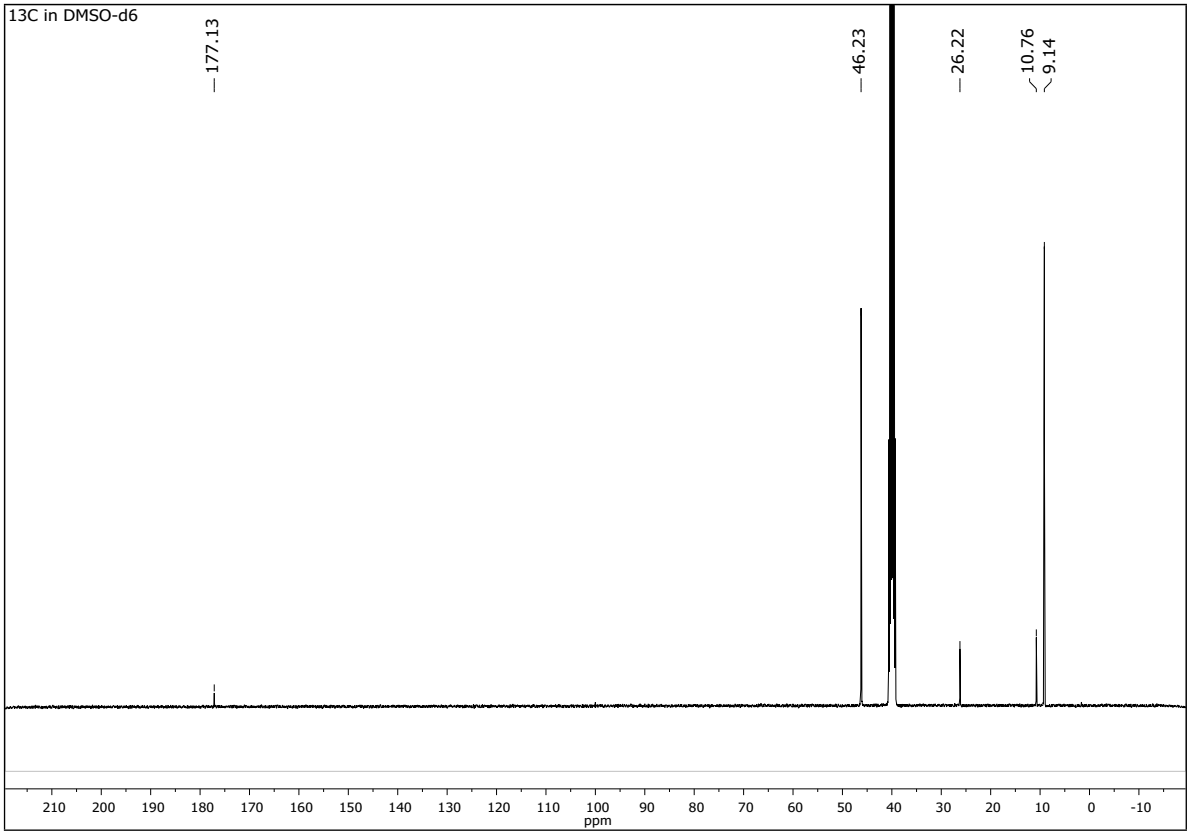

^{13}C - NMR spectrum of [**6**]$(NHEt_3)_2$ in DMSO-d_6

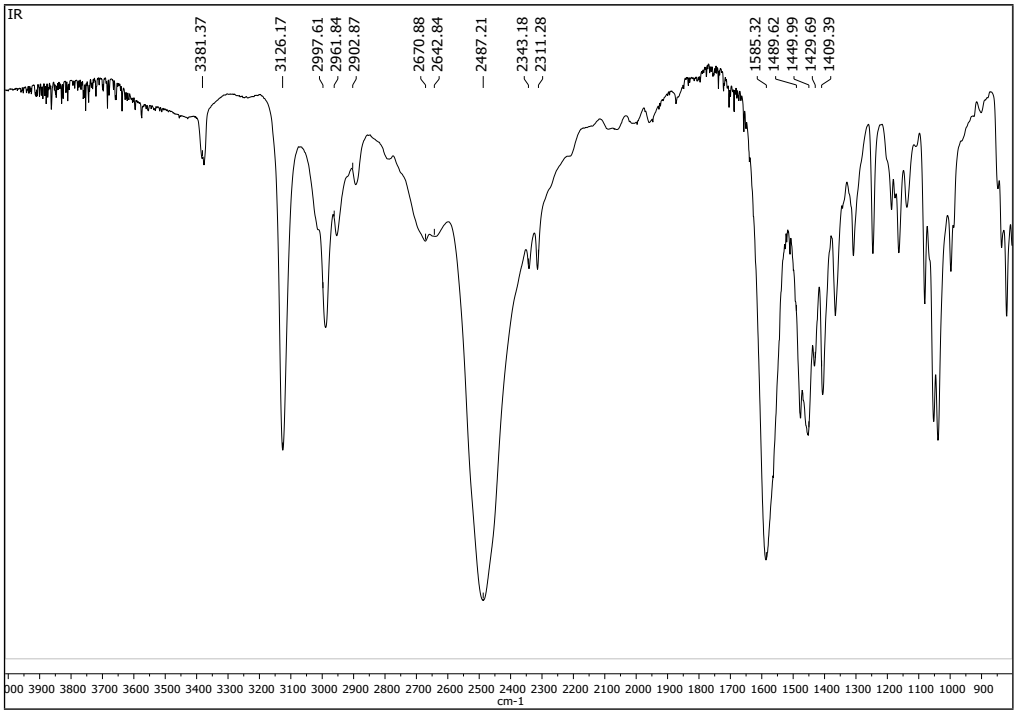

IR - spectrum of [**6**]$(NHEt_3)_2$ in KBr

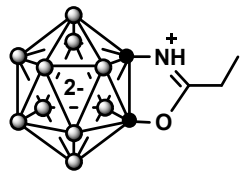

[8]NHEt$_3$

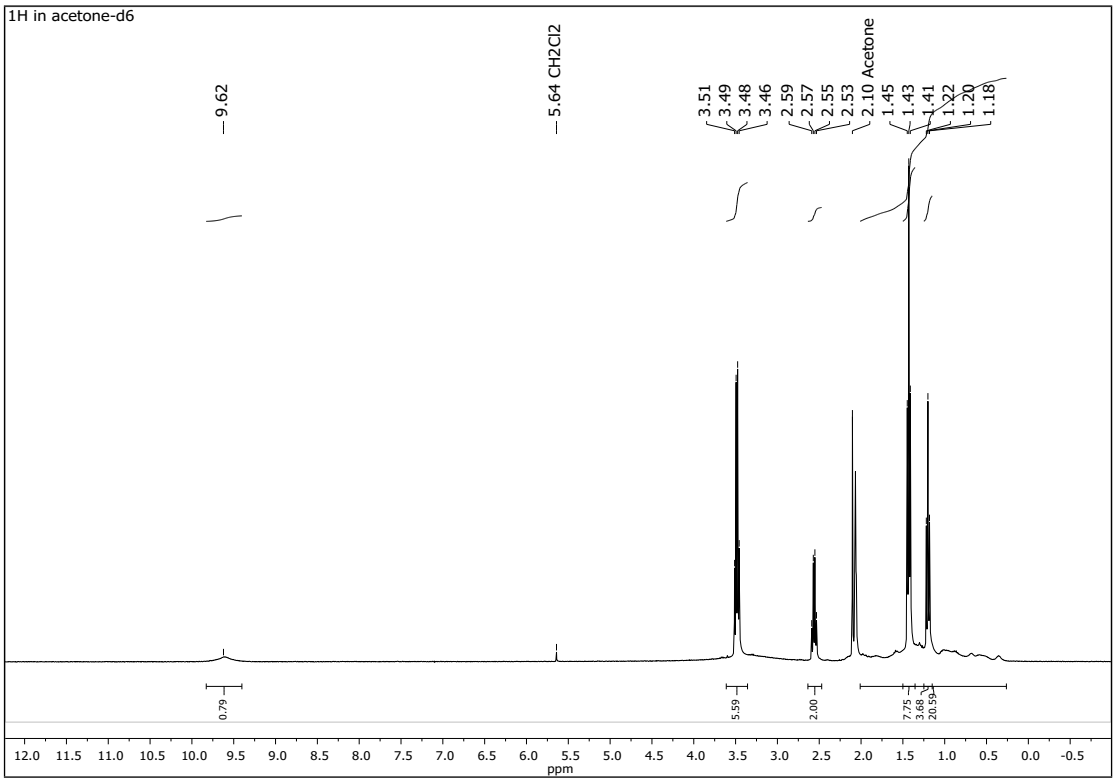

^{1}H - NMR spectrum of [**8**]NHEt$_3$ in acetone-d$_6$

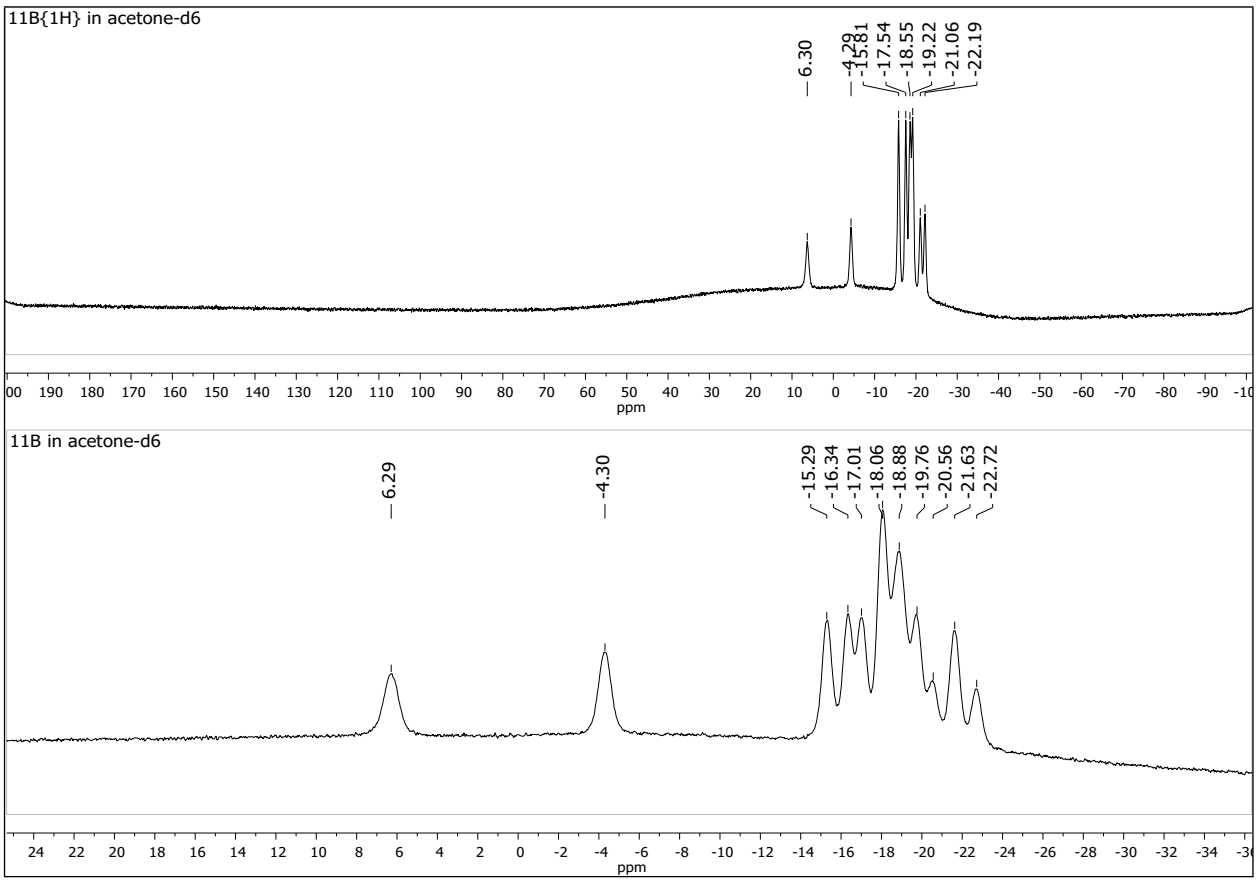

$^{11}B\{^{1}H\}$- and ^{11}B - NMR spectra of [**8**]$NHEt_3$ in acetone-d_6

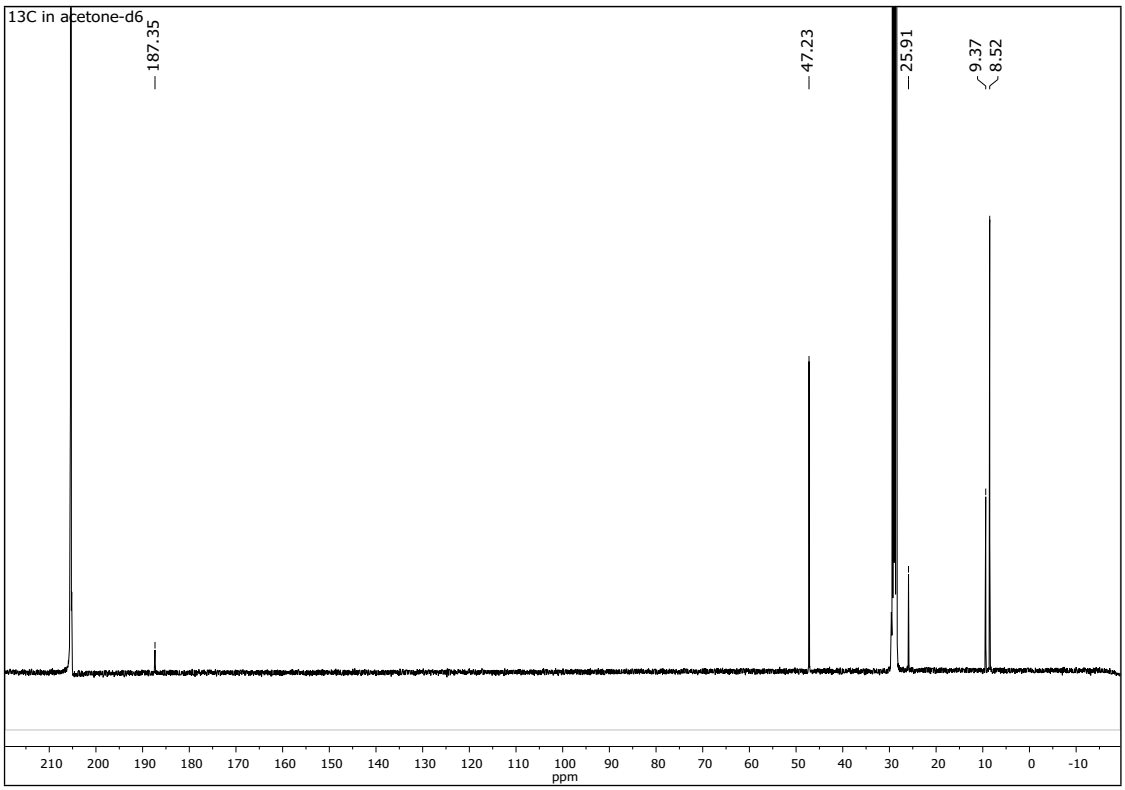

^{13}C - NMR spectrum of [**8**]$NHEt_3$ in acetone-d_6

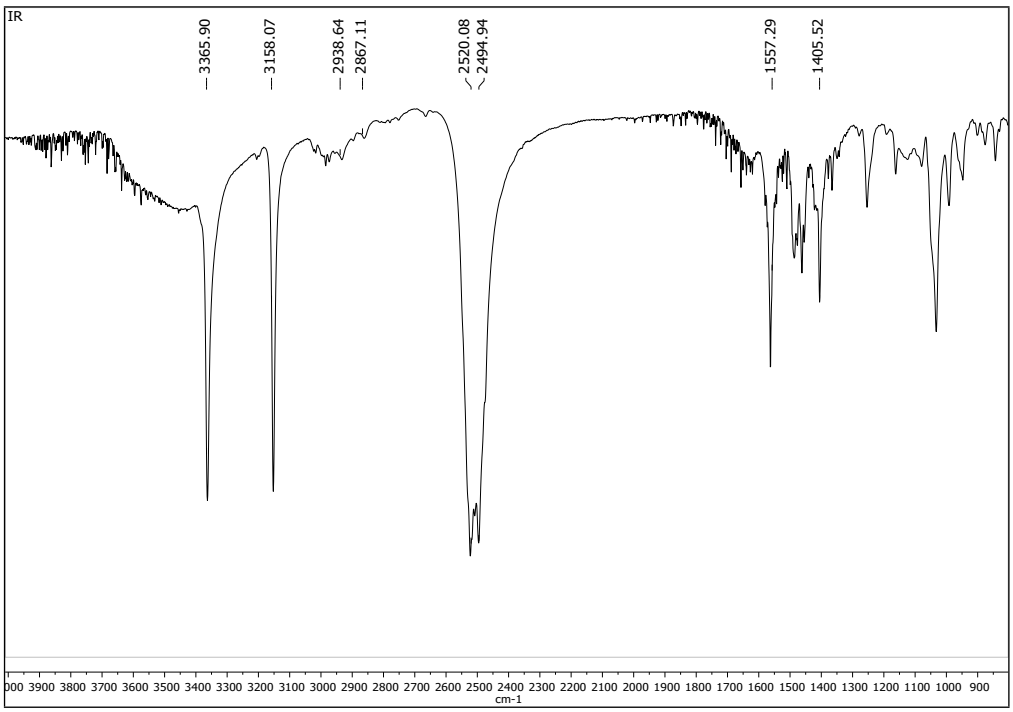

IR - spectrum of [**8**]$NHEt_3$ in KBr

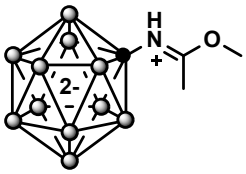

[9]$NHEt_3$

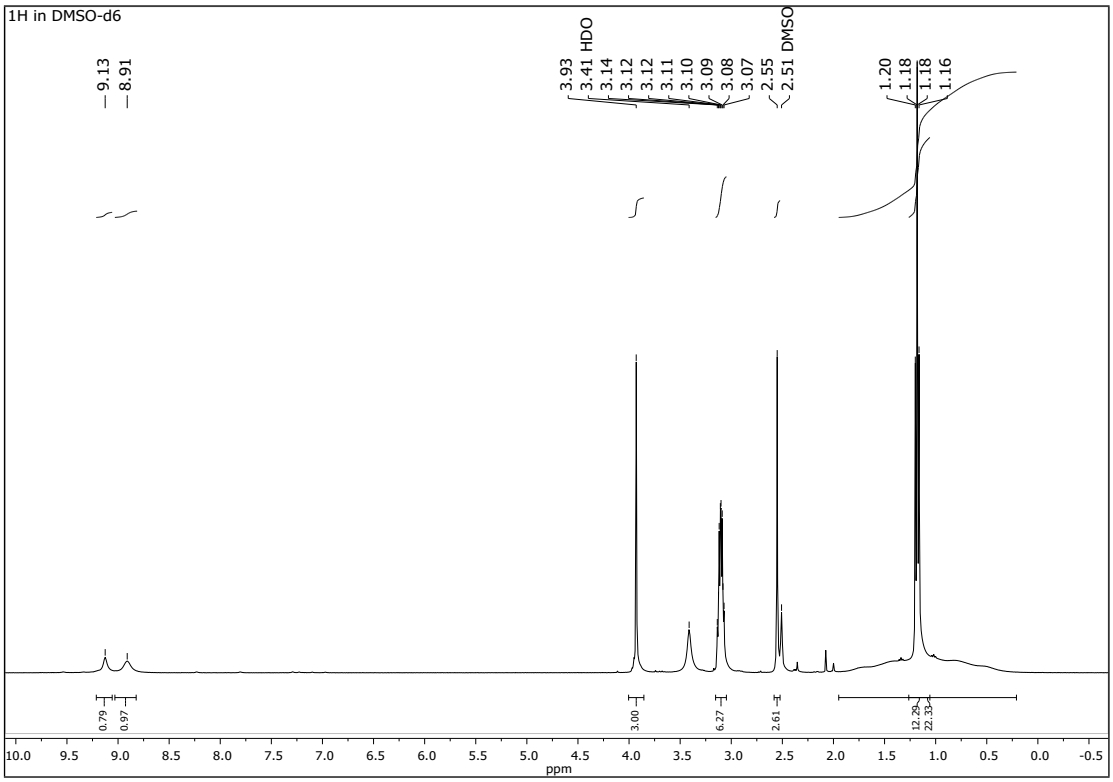

^{1}H - NMR spectrum of [**9**]$NHEt_3$ in DMSO-d_6

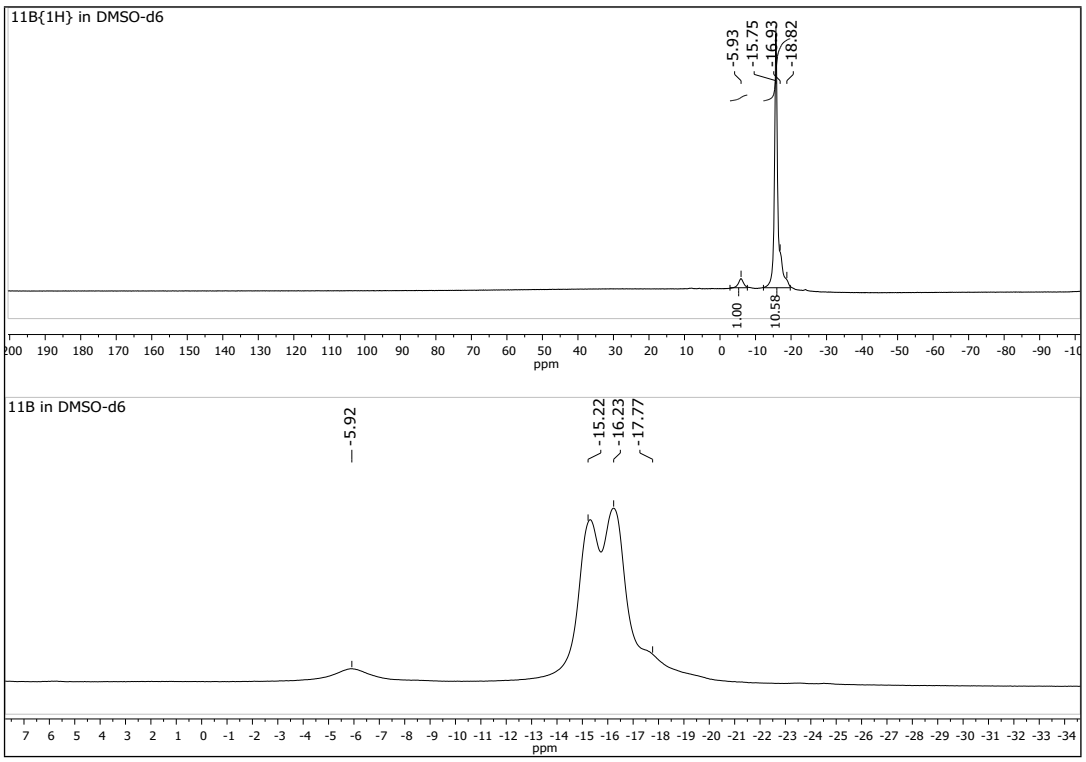

$^{11}B\{^{1}H\}$- and ^{11}B - NMR spectra of [**9**]$NHEt_3$ in DMSO-d_6

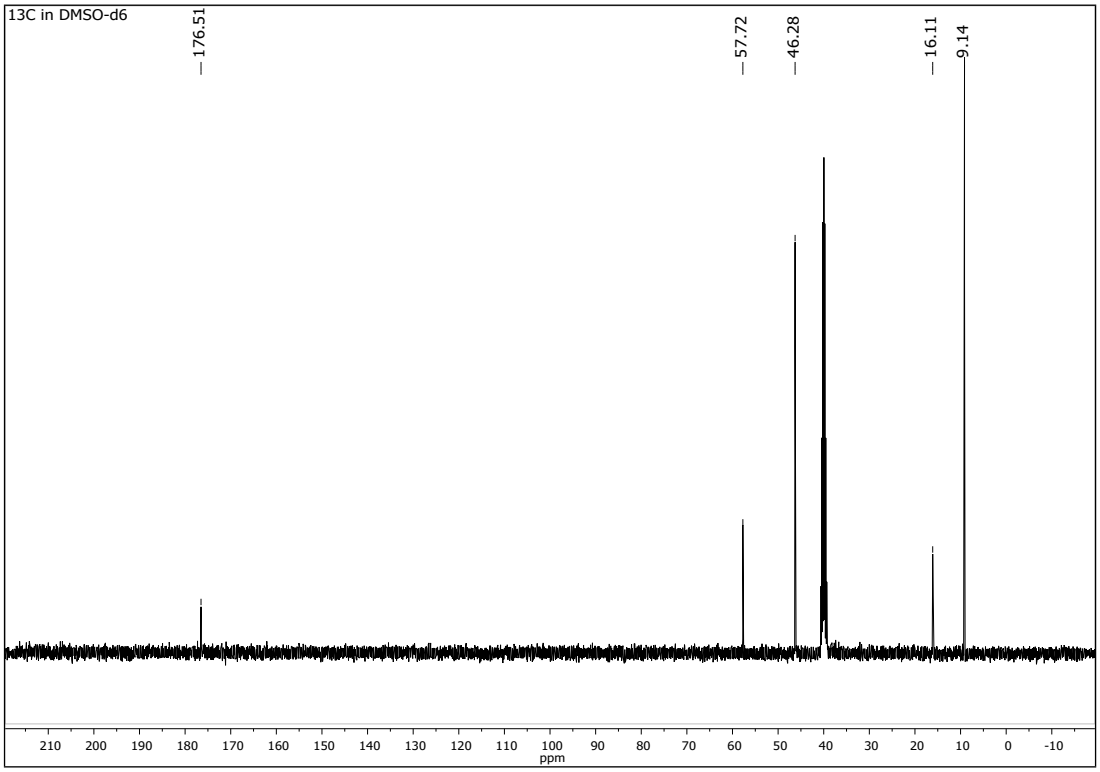

^{13}C - NMR spectrum of [**9**]$NHEt_3$ in DMSO-d_6

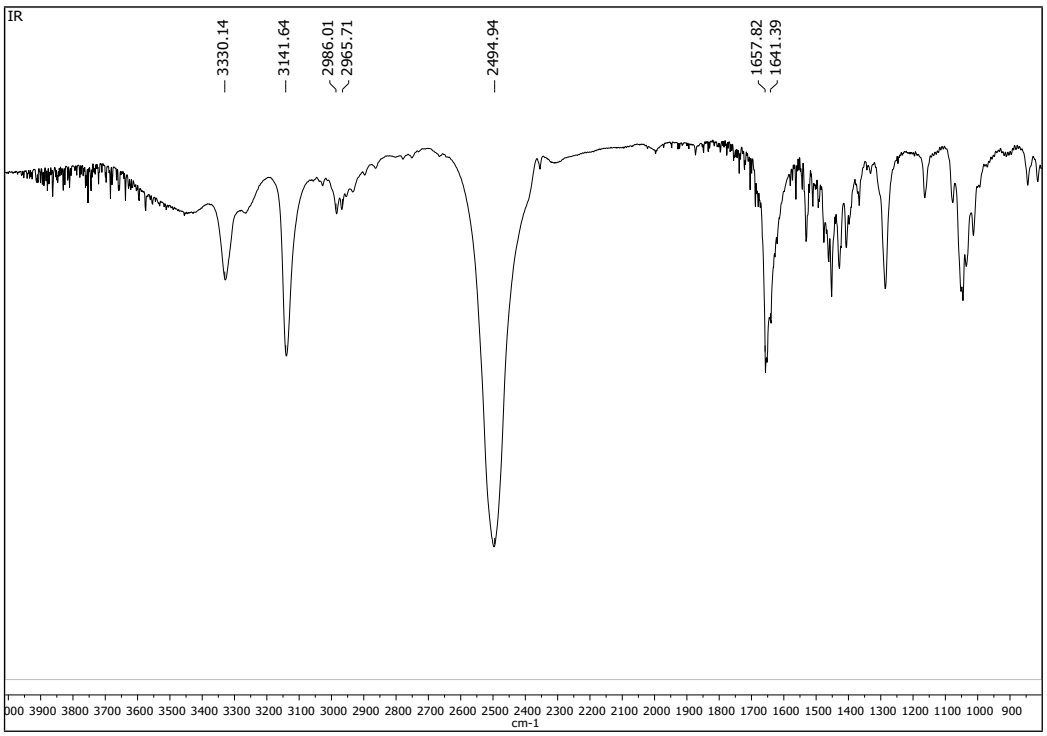

IR - spectrum of [**9**]$NHEt_3$ in KBr

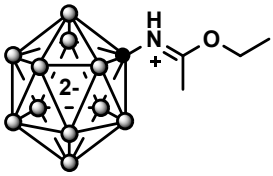

[10]$NHEt_3$

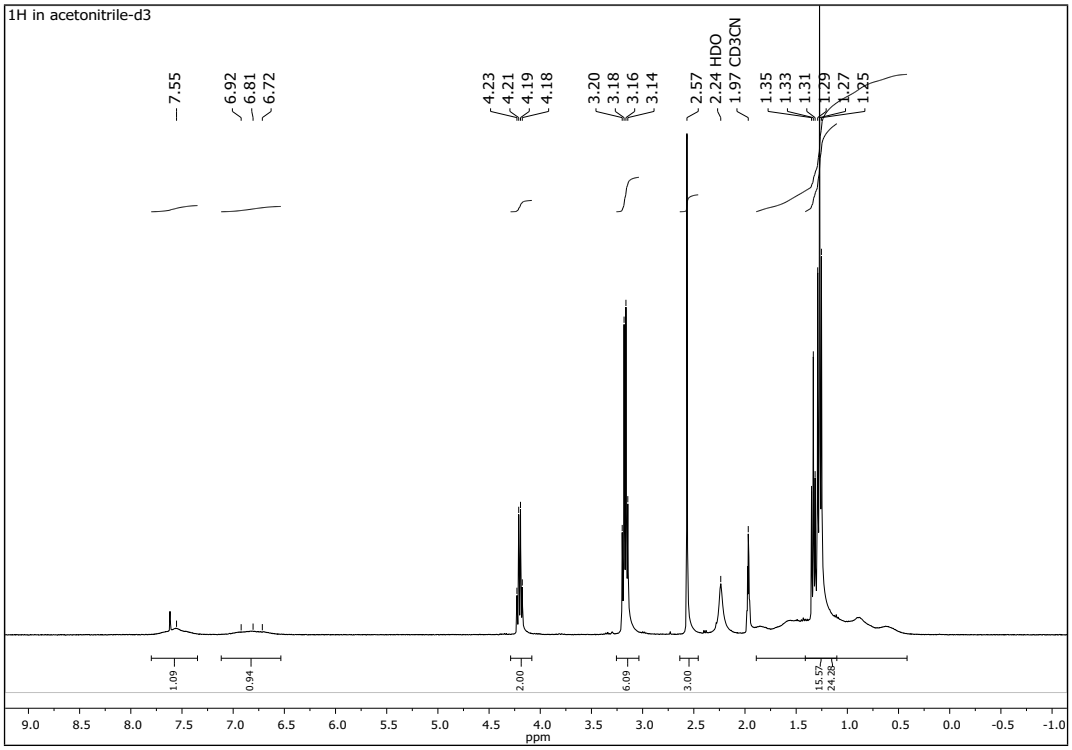

^{1}H - NMR spectrum of [**10**]$NHEt_3$ in acetonitrile-d_3

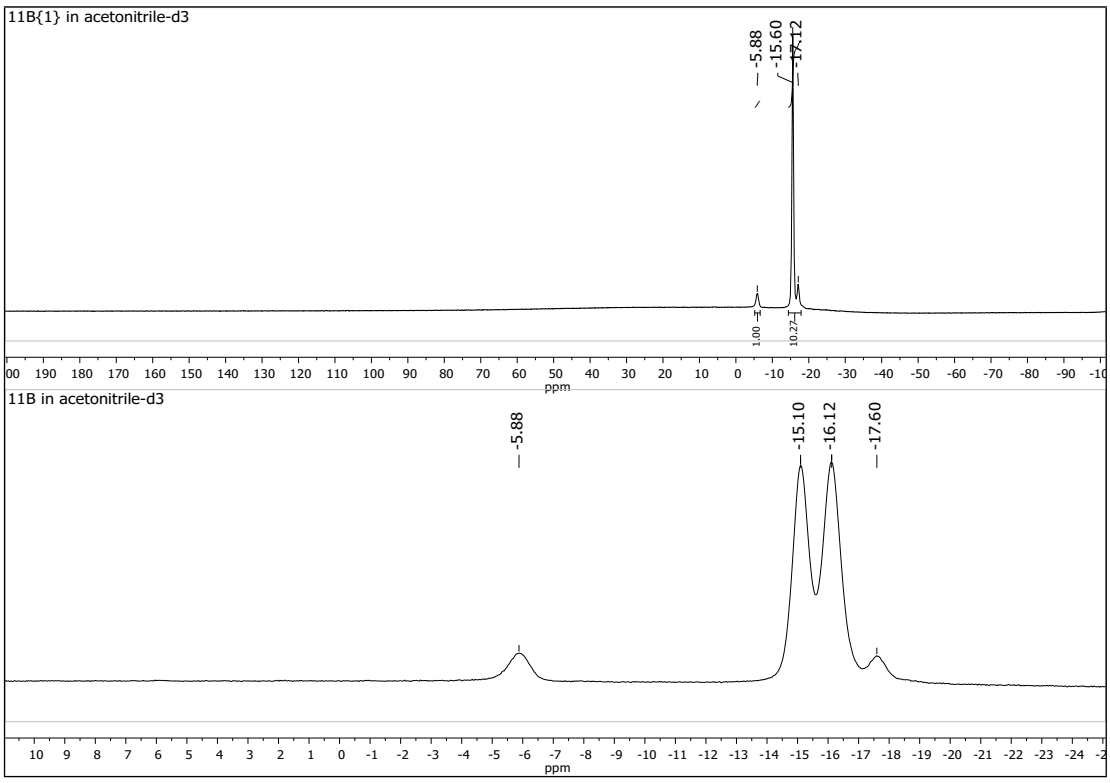

$^{11}B\{^{1}H\}$- and ^{11}B - NMR spectra of [**10**]$NHEt_3$ in acetonitrile-d_3

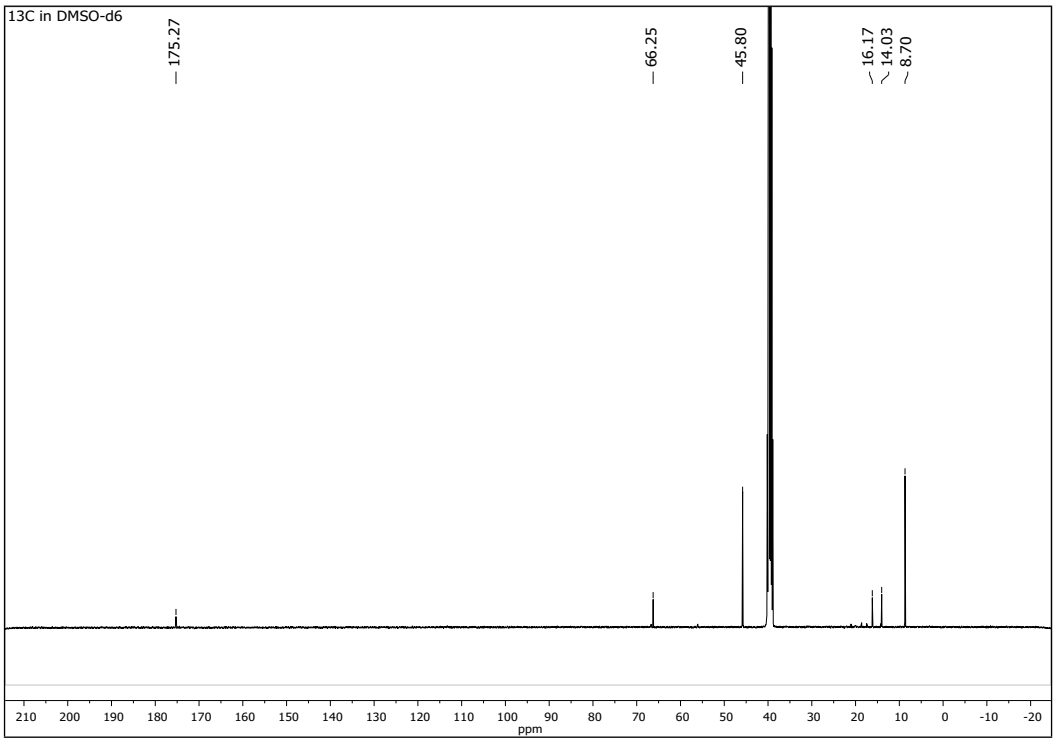

^{13}C - NMR spectrum of [**10**]$NHEt_3$ in DMSO-d_6

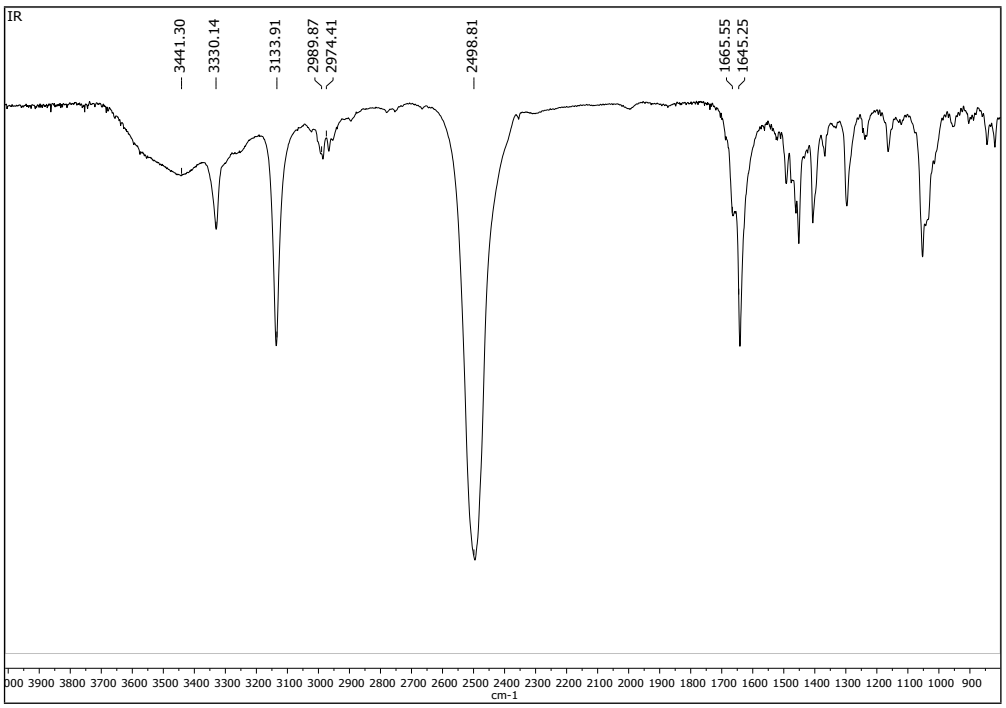

IR - spectrum of [**10**]$NHEt_3$ in KBr

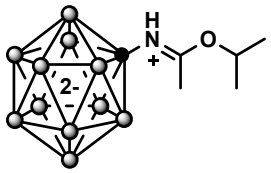

[11]$NHEt_3$

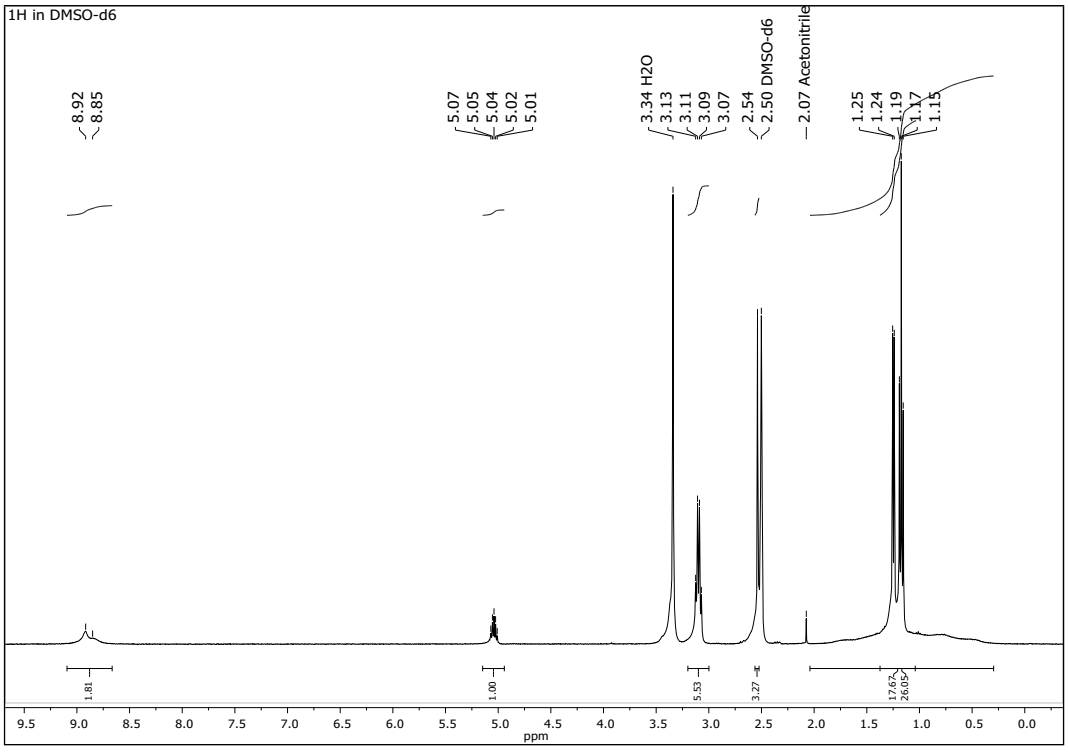

^{1}H - NMR spectrum of [**11**]$NHEt_3$ in DMSO-d_6

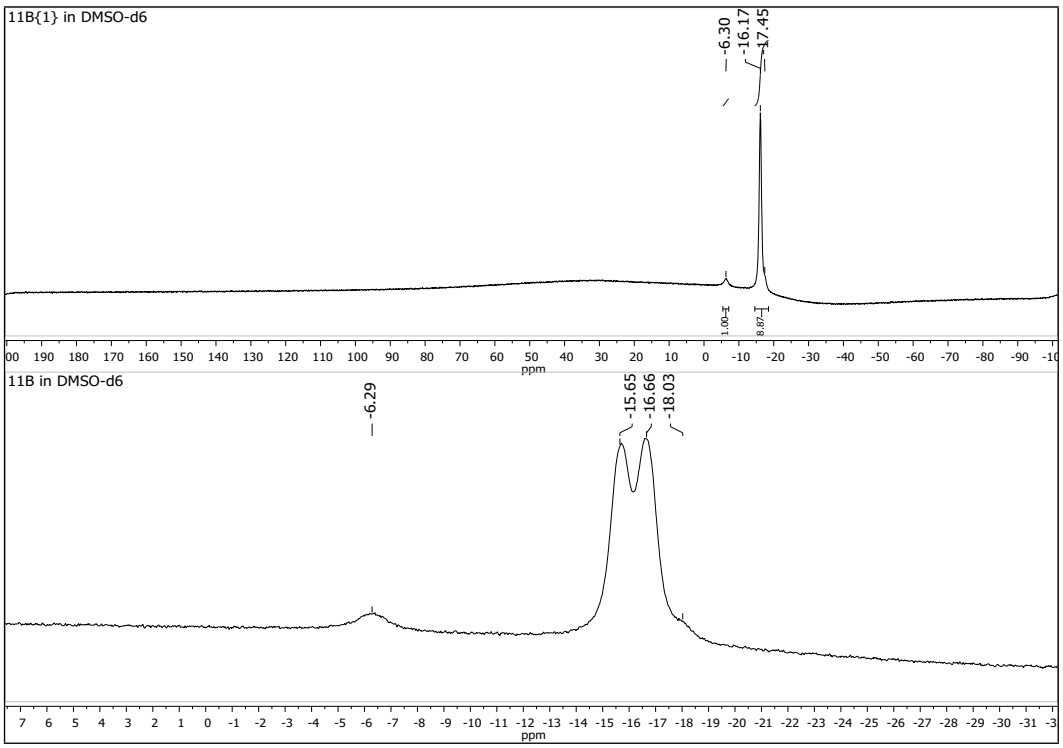

$^{11}B\{^{1}H\}$- and ^{11}B - NMR spectra of [**11**]$NHEt_3$ in DMSO-d6

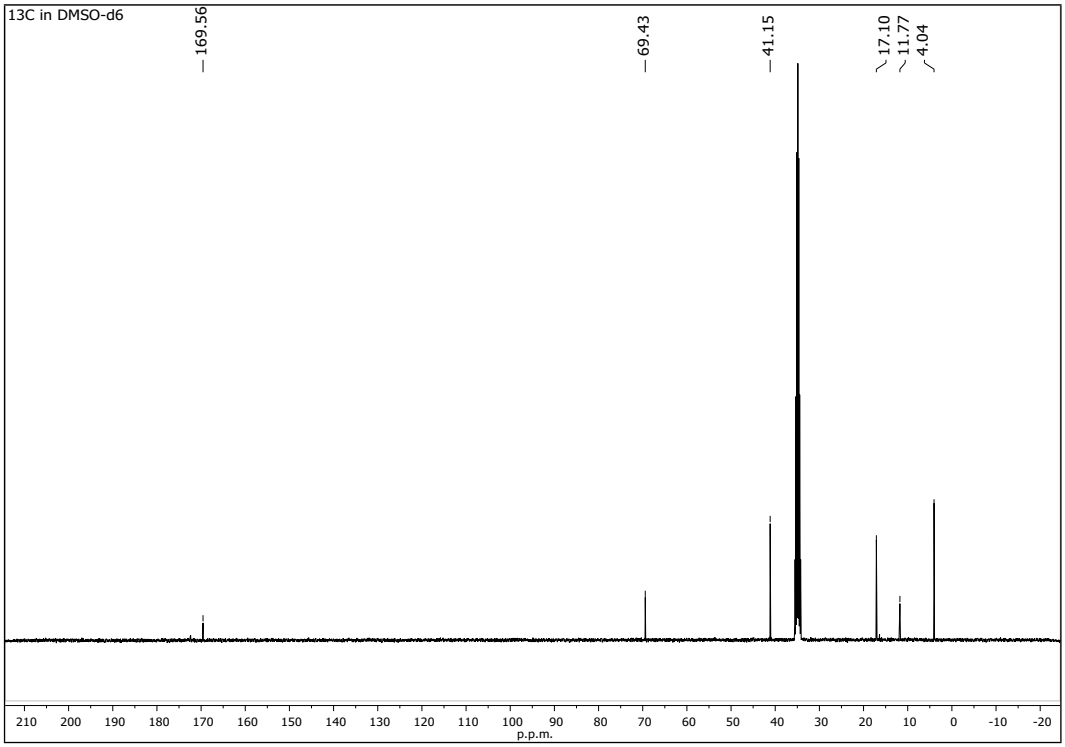

^{13}C - NMR spectrum of [**11**]$NHEt_3$ in DMSO-d_6

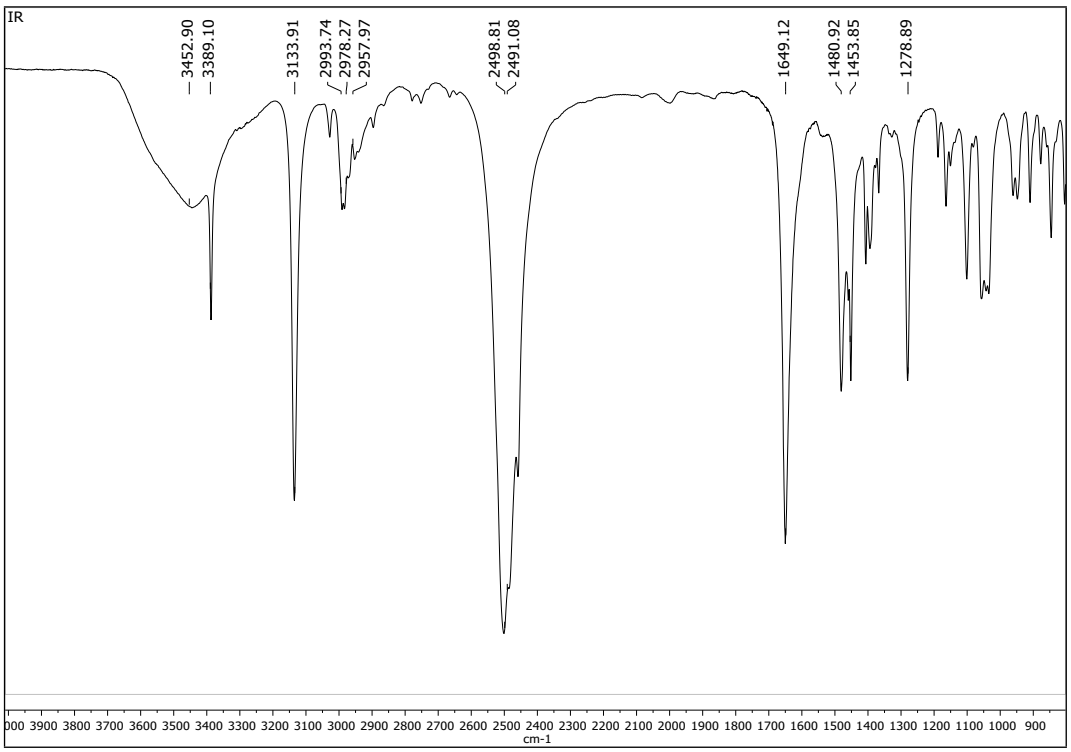

IR - spectrum of [**11**]$NHEt_3$ in KBr

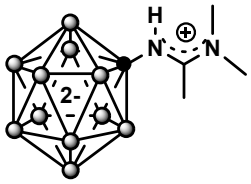

[12]NH_2Me_2 and [12]Cs

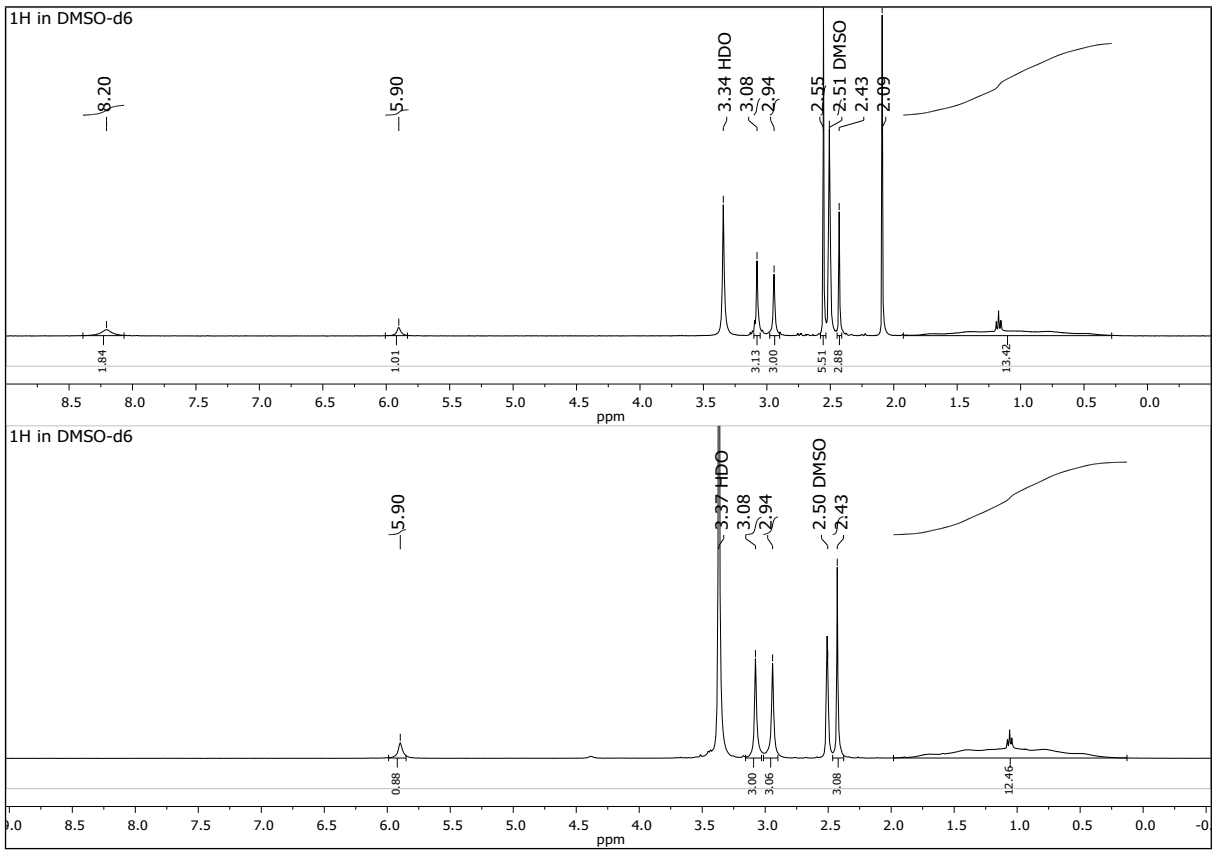

^{1}H - NMR spectra of [**12**]NH_2Me_2 on the top and [**12**]Cs on the bottom in DMSO-d_6

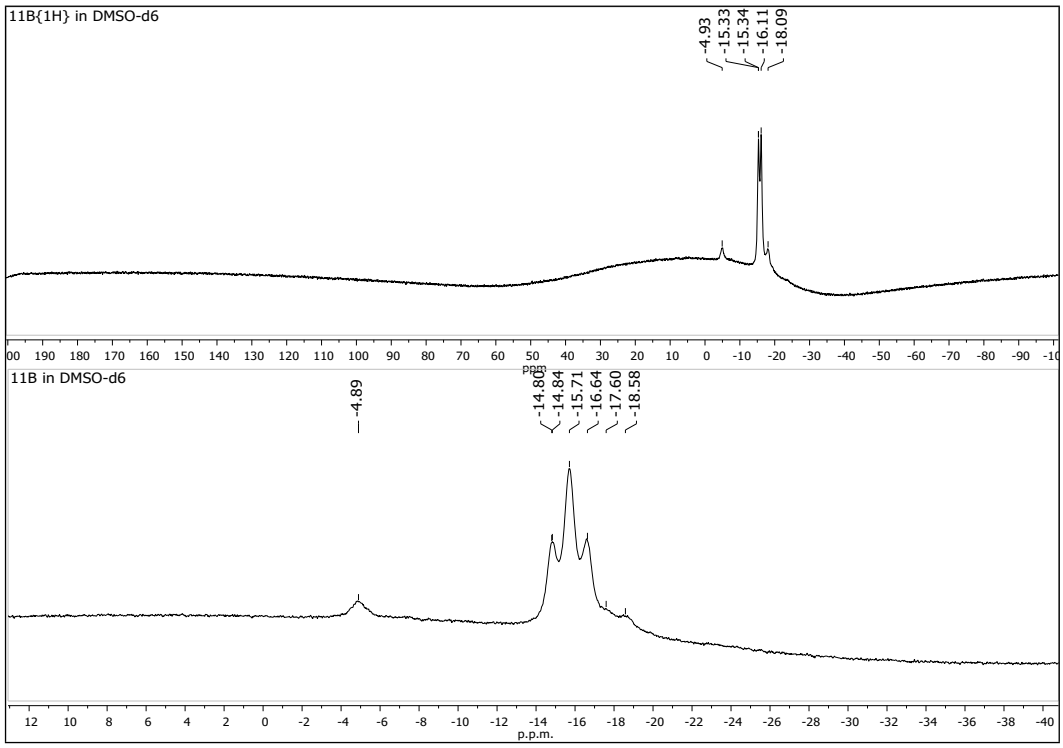

^{11}B{^{1}H} – and ^{11}B spectra of [**12**]Cs in DMSO-d_6

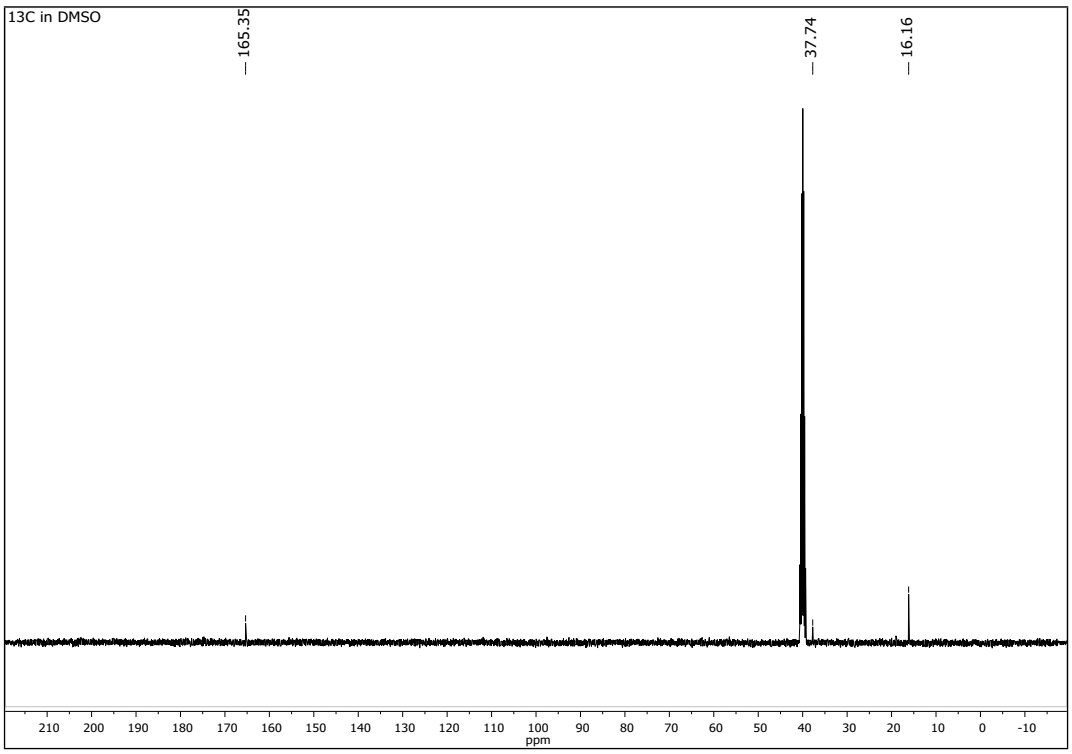

^{13}C - NMR spectrum of [**12**]Cs in DMSO-d_6

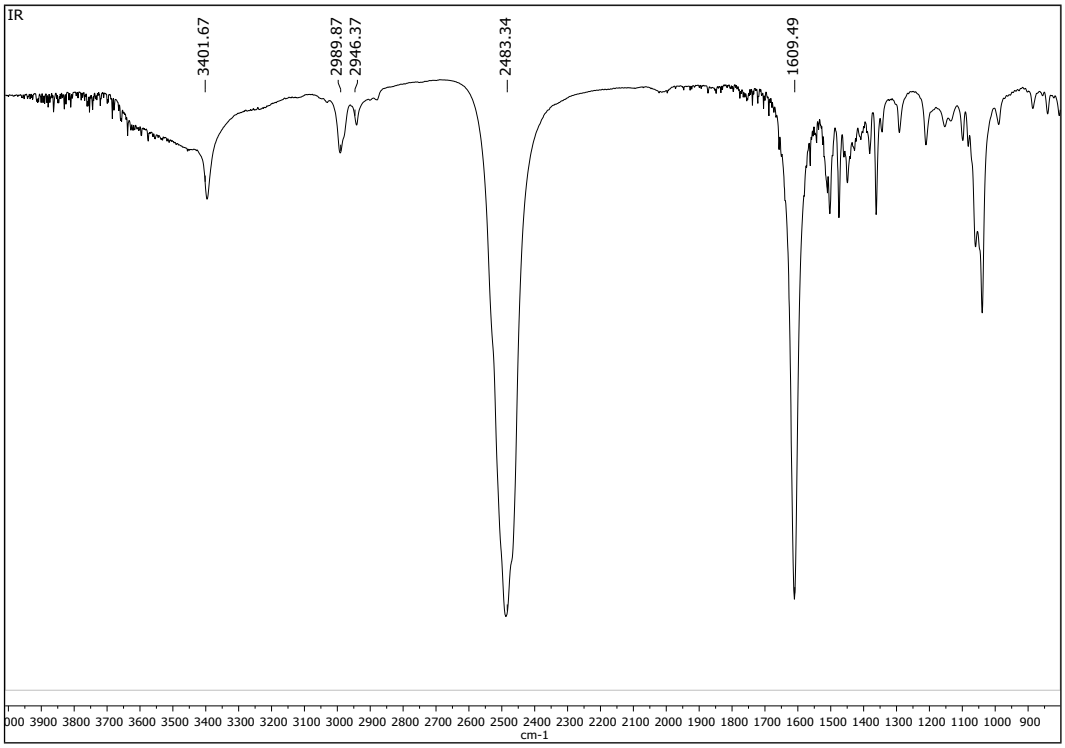

IR spectrum of [**12**]Cs in KBr

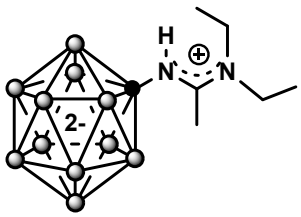

[13]NH_2Me_2 and [13]Cs

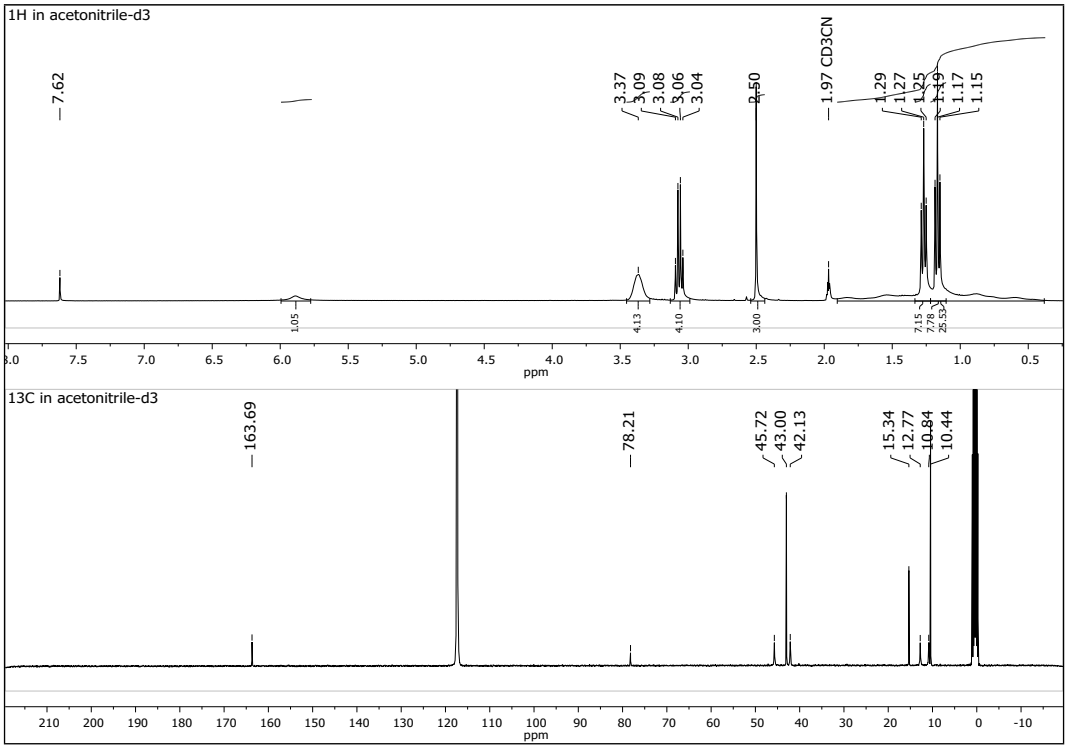

^1H – and ^{13}C-NMR spectra of [**13**]NH_2Et_2 in acetonitrile-d_3

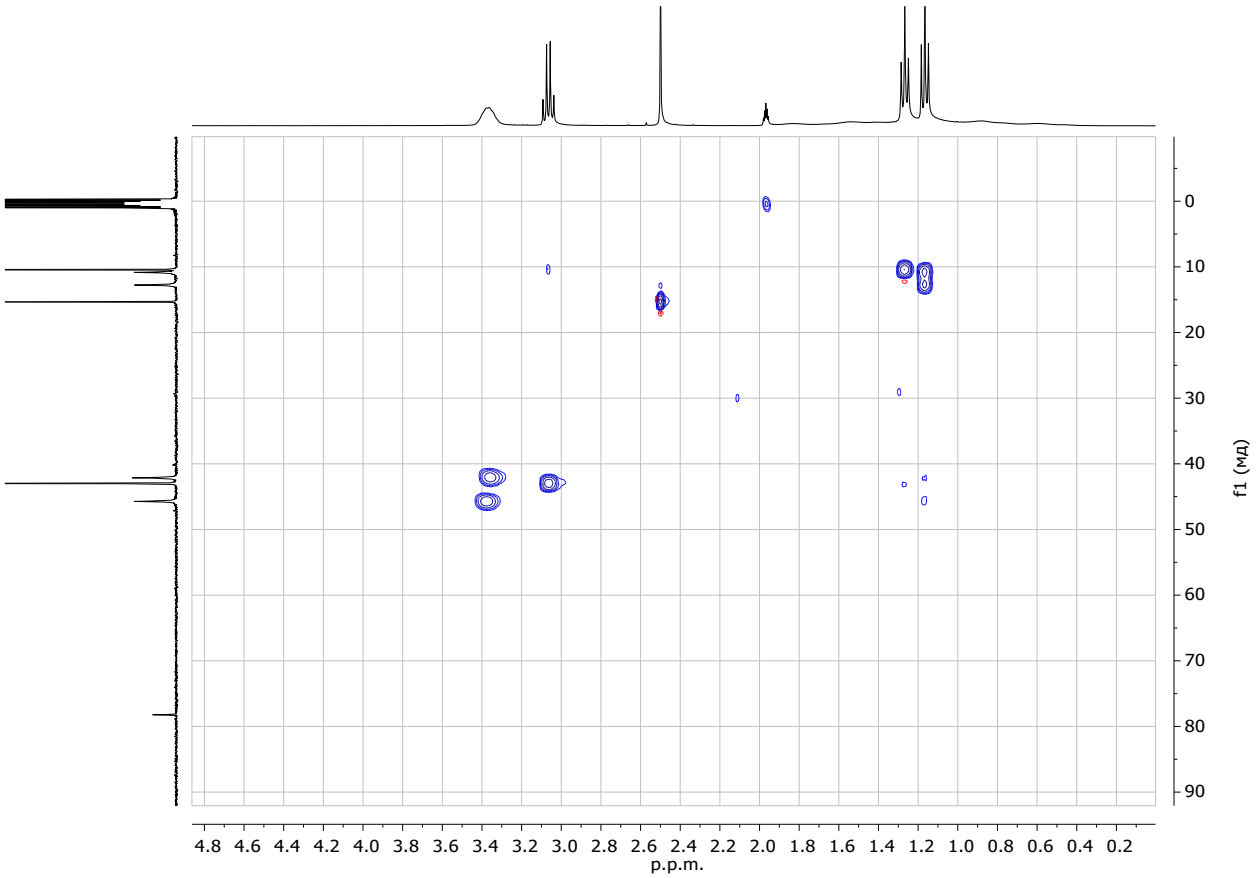

^{1}H-^{13}C HSQC NMR of [**13**]NH_2Et_2 in acetonitrile-d_3

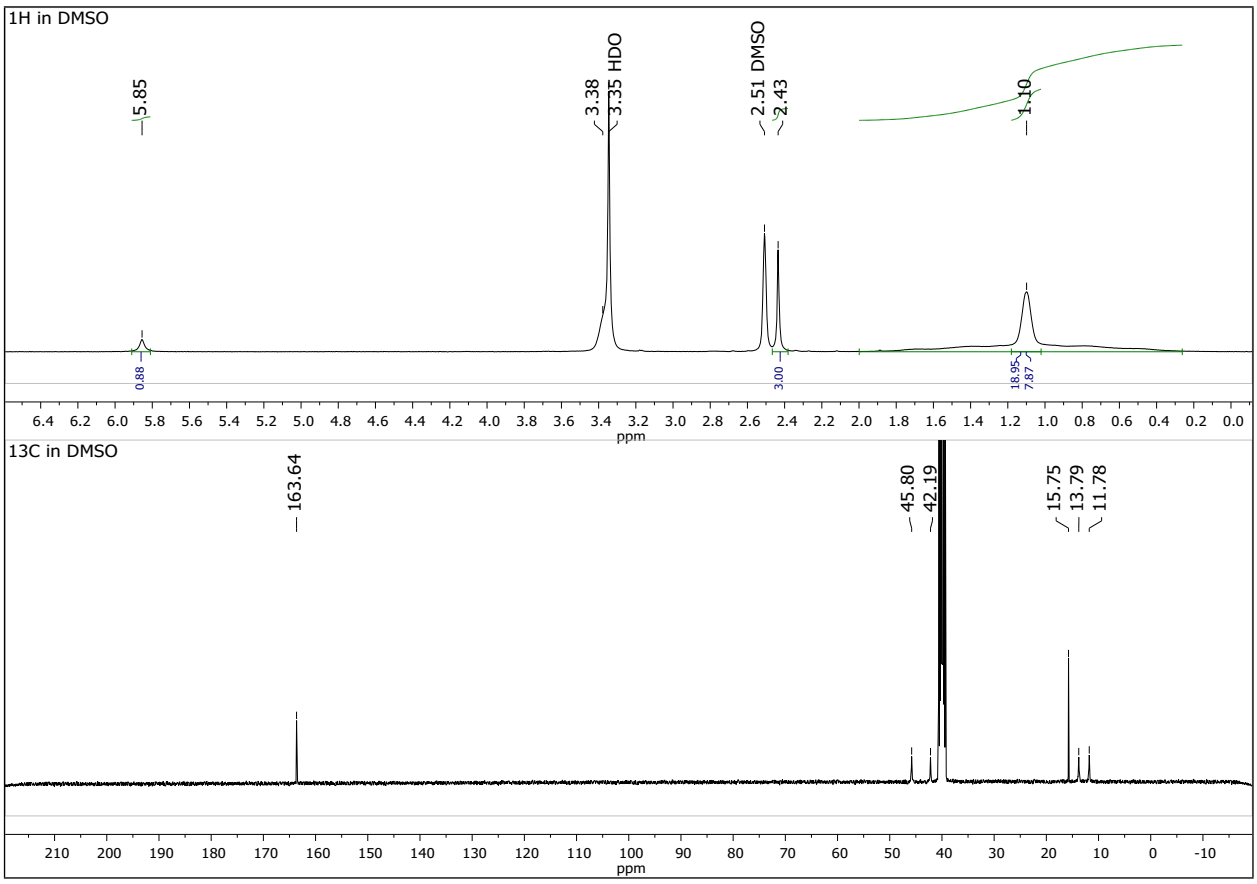

^{1}H – and ^{13}C-NMR spectra of [**13**]Cs in DMSO-d$_6$

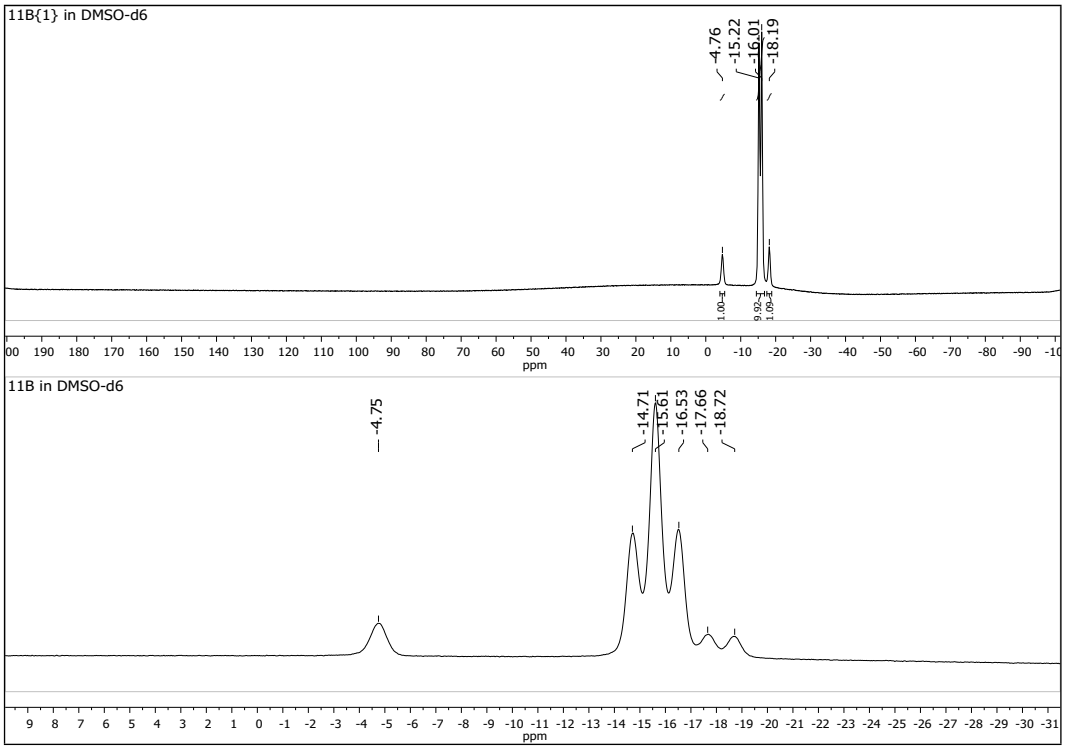

^{11}B{^{1}H} – and ^{11}B spectra of [**13**]Cs in DMSO-d$_6$

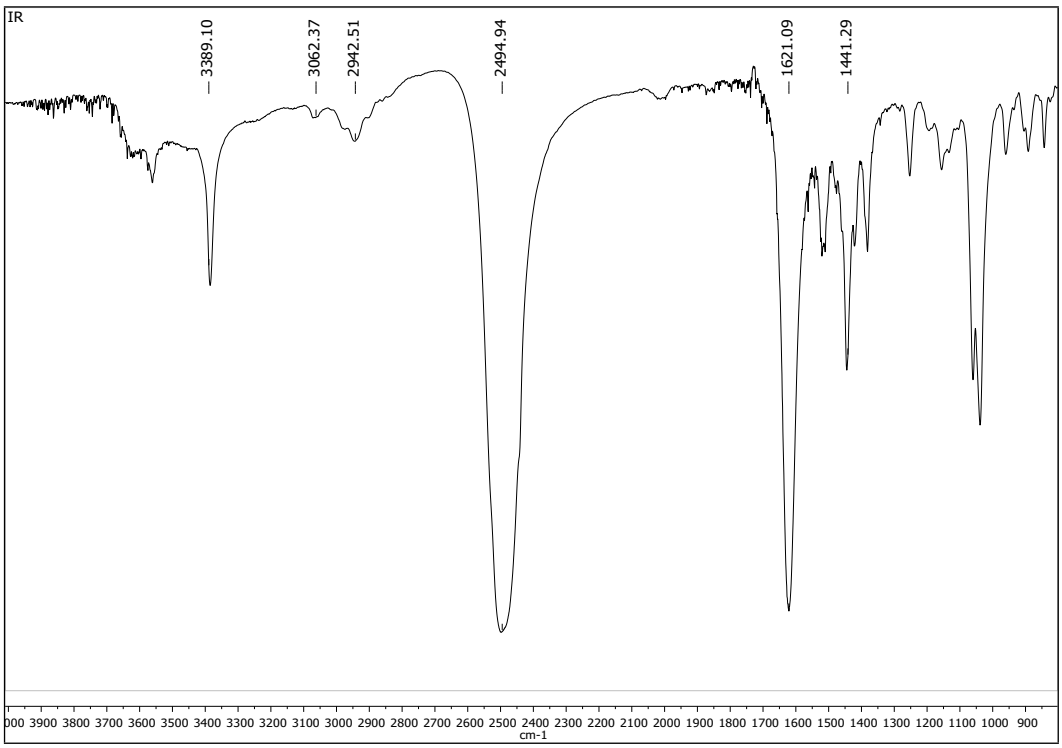

IR spectrum of [**13**]Cs in KBr

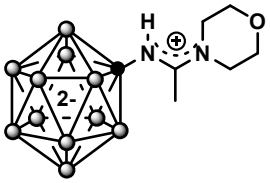

[14]$NH_2(CH_2CH_2)_2O$ and [14]Cs

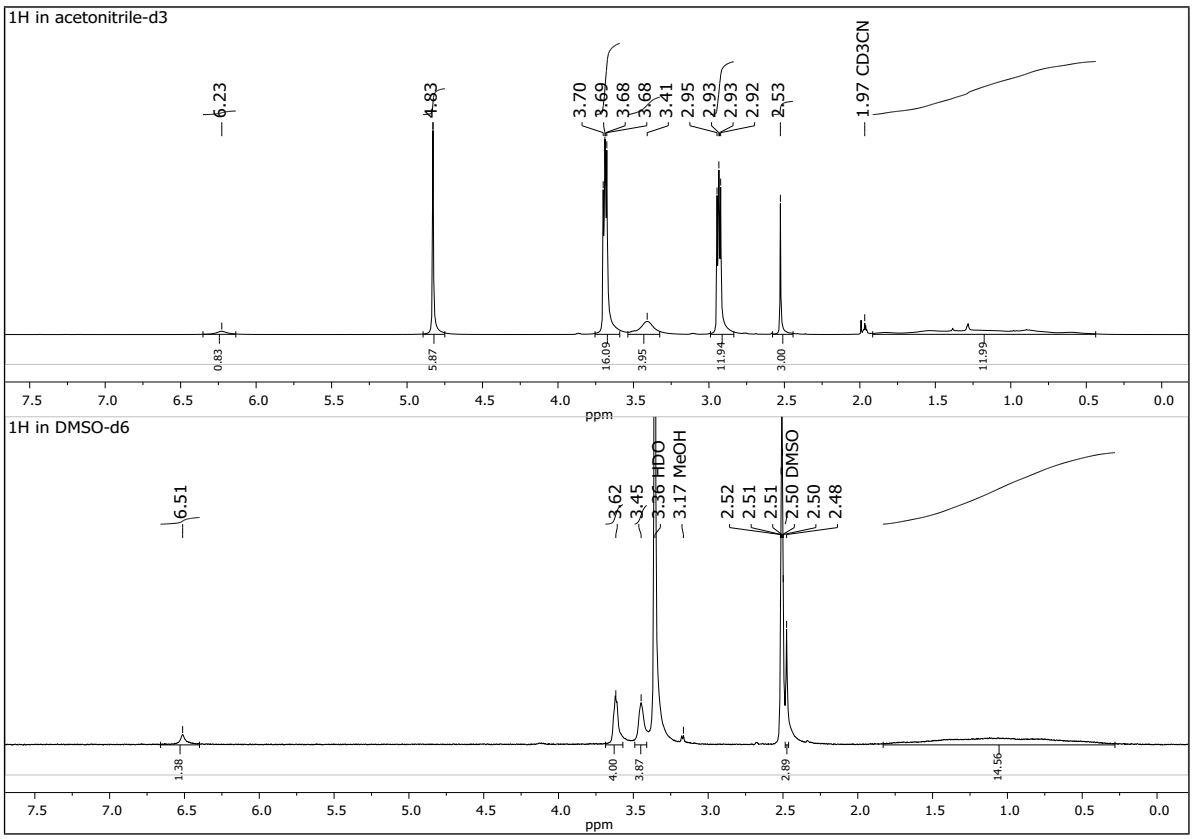

^{1}H-NMR spectrum of [**14**]$NH_2(CH_2CH_2)_2O$ in acetonitrile-d_3 on the top and ^{1}H-NMR spectrum of [**14**]Cs in DMSO-d_6 on the bottom

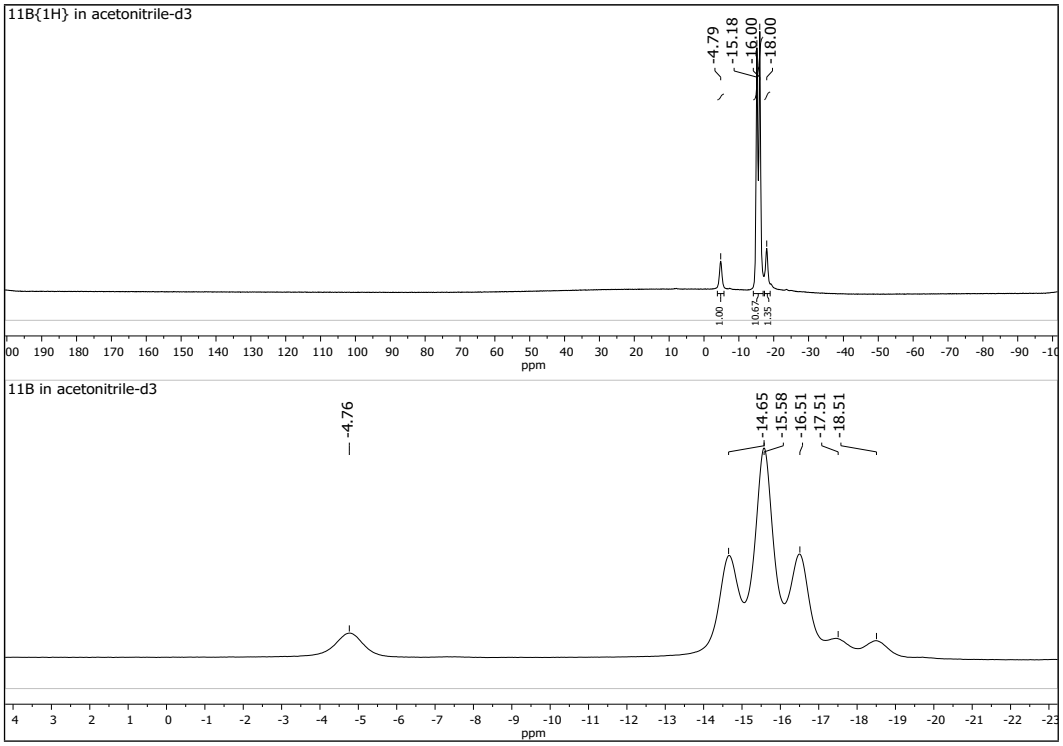

^{11}B{^{1}H} – and ^{11}B - NMR spectra of [**14**]$NH_2(CH_2CH_2)_2O$ in acetonitrile-d_3

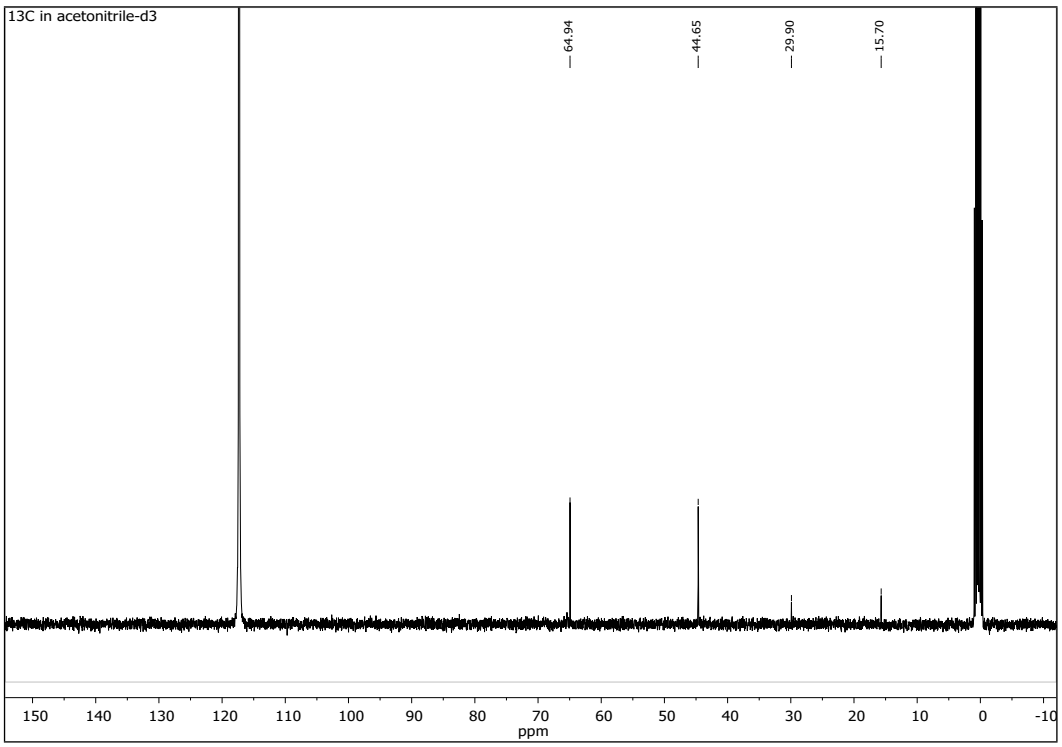

^{13}C - NMR spectrum of [**14**]$NH_2(CH_2CH_2)_2O$ in acetonitrile-d_3

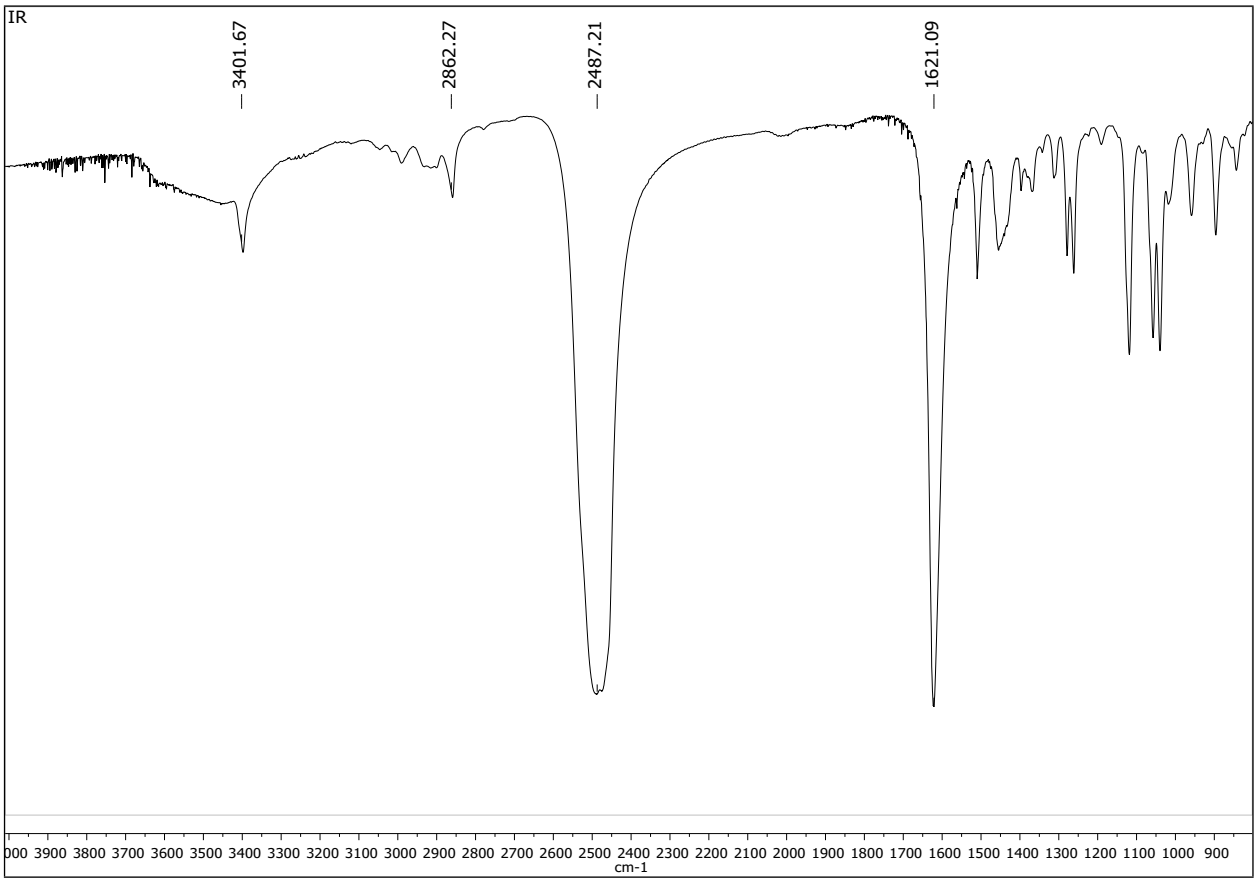

IR spectrum of [**14**]Cs in KBr

II Acid-assisted nucleophilic substitution mechanism

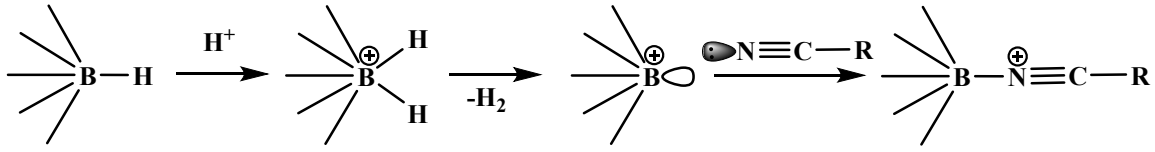

Scheme S1.

III Figure S1

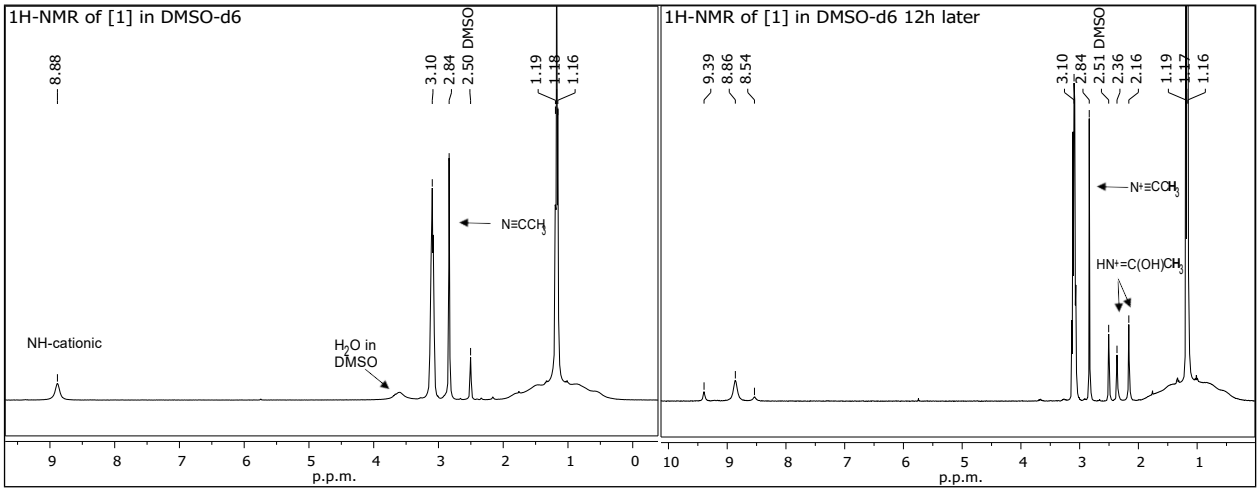

Figure S1. Experiment in the NMR tube. 50 mg of [**1**] dissolved in 0.5 ml of DMSO-*d6*. ^{1}H-NMR spectra.

IV X-ray crystallography and DFT calculation

Table S1. Crystallography data and refinement details for [**11**]×acetone and [**14**]×acetone.

	[**11**]×acetone	[**14**]×acetone
Formula	$C_{14}H_{44}B_{12}N_2O_2$	$C_{17}H_{48}B_{12}N_4O_4$
Mass	402.23	502.31
T, K	120	100
Crystal system	Triclinic	Monoclinic
Space group	P-1	$P2_1/n$
Z	2	4
a, Å	8.9565(4)	8.5596(2)
b, Å	10.4887(5)	21.4218(4)
c, Å	13.7458(7)	15.3224(3)
a, °	79.917(2)	90
b, °	89.741(2)	93.2185(8)
g, °	82.490(2)	90
V, Å^3	1260.24(10)	2805.11(10)
d_{calc}, gЧcm^{-3}	1.060	1.189
F(000)	436	1080
$2q_{max}$, °	58	60
Number of reflections measured	19435	57615
Independent reflections	6033	8215
Reflections with I>2s(I)	3573	5806
Number of parameters	410	420
R_1	0.0530	0.0482

wR_2	0.1320	0.1402
GOF	0.967	1.010
Residual electron density, $eЧÅ^{-3}(d_{min}/d_{max})$	0.210/-0.240	0.297/-0.342

The DFT calculations were performed using the Gaussian 09 program[1] (rev. D01) at the PBE0[2,3]/6-311++G(d,p) level with the Grimme's D3 dispersion corrections and Becke-Jonson damping.[4] Standard convergence criteria were used for the optimization procedures and relaxed scans. Equilibrium structures of both compounds correspond to minimums on potential energy surface according to the calculations of Hessian of electronic energy (ultrafine grids, no imaginary modes were found). The MultiWFN[5] and AIMAll[6] programs were used to analyze metrics defined in the real space (electron density function, source function, reduced density gradient). The NBO populations were calculated using the NBO 3.1 program.[7]

Crystal structure of [11]NHEt$_3$×acetone.

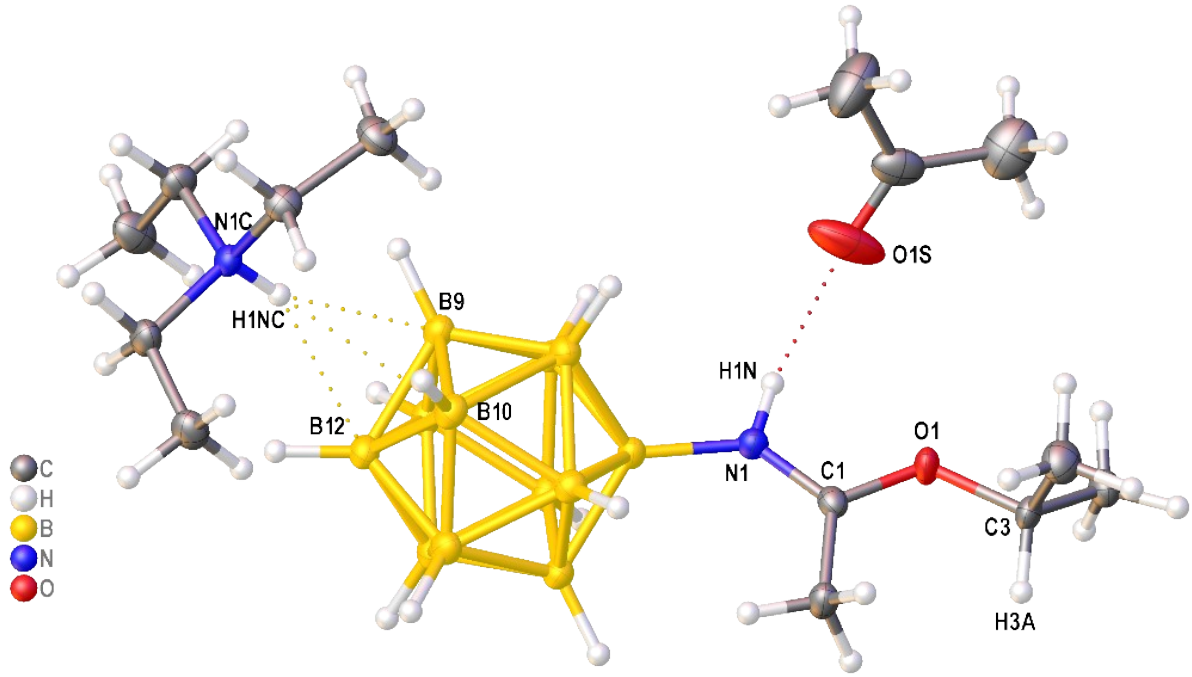

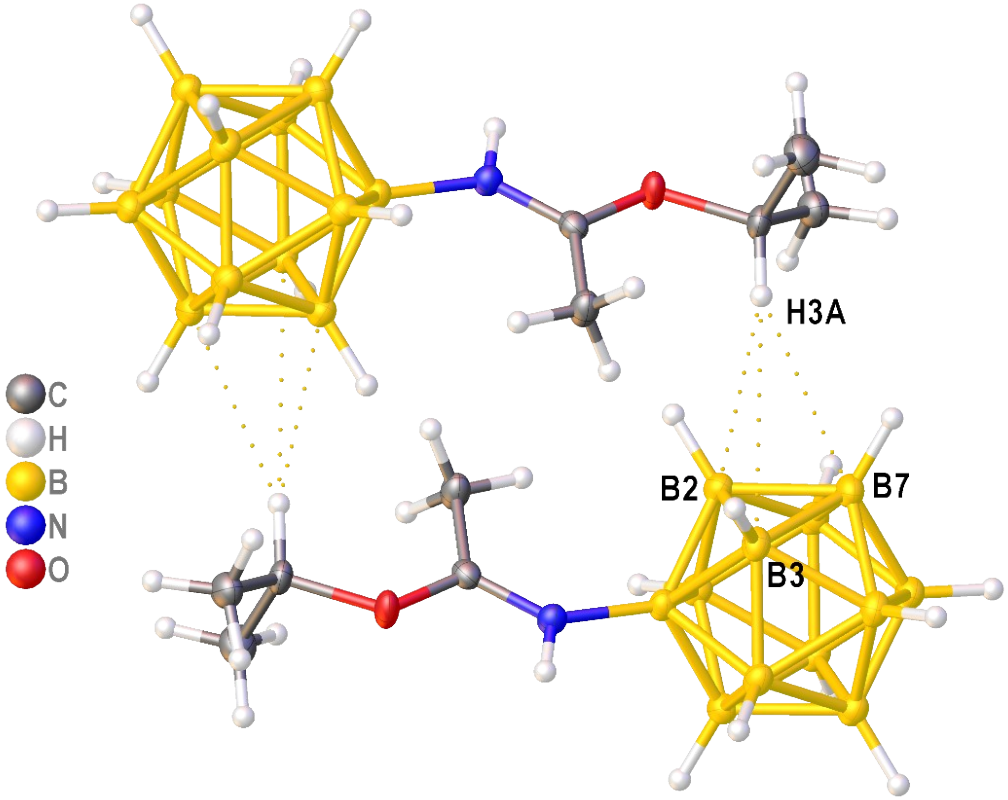

Figure S2. The independent unit of [**11**]·acetone crystal (top) and centrosymmetric dimers of [**11**] anions in crystal (bottom) with the representation of non-hydrogen atoms by probability ellipsoids of atomic displacements (p=0.5). Dotted lines correspond to non-covalent interactions discussed in the main text.

The structure of the anion in [**11**]×acetone crystals is expected for this class of compounds and very similar to the known benzoylimido-dodecaborate.[8] For instance, the C1-N1 bond length equals to 1.296(2) Å that agrees well with the formal double-bonding character of this bond. The conformation of the isopropyloxy substituent probably serves as the only interesting feature of the anion structure. Namely, a rather large rotation of the isopropyl function against the O1-C3 bond is observed (the C1-O1-C3-H3A torsion angle equals to 34.6°). This feature can be rationalized by the combination of anomeric effects and intermolecular forces. The charge transfer from oxygen lone electronic pairs towards the σ*-orbital of the C3-H3A bond can be supposed using the geometric criteria: the effective position of one of the lone pairs of O1 is nearly antiperiplanar to the C3-H3A bond (the corresponding torsion angle equals to 158°). However, the corresponding charge transfer energy is only 4.1 kcal·mol^{-1} as revealed by the NBO analysis[9] for the anion calculated by DFT with partial optimization of only hydrogen atoms. At the same time, the H3A atom, formally being of acidic character, is involved in shortened contacts with the B2(H)-B3(H)-B7(H) face of borane cage of neighboring anion (Figure 2, bottom): the H3A…B distances are 3.049, 3.103 and 3.174 Å, the angle between C3-

H3A bond and centroid of the borane face is 139.9° (intramolecular C-H bond lengths were normalized). Bounding anions into centrosymmetric dimers, the corresponding CH…H_3B_3 interactions may serve as additional factor stabilizing the conformation of isopropyloxy substituent. Indeed, while the C1-O1-C3-H3A torsion angle in the isolated optimized anion is 41.6°, it becomes very close to the experimental value in the corresponding optimized dimer (33.9°).

Two more types of intermolecular interactions in the island-type crystal packing of [**11**]×acetone should be especially mentioned. The solvate acetone molecule is mainly retained by the H-bond formed by its oxygen atom and the NH fragment of the anion. This H-bond can be attributed to weak ones (N1…O1S 2.883(2) Å, the N1-H1N-O1S angle equals to 155.7° with the N1-H1N bond length being normalized) that is in line with large displacements parameters of the O1S atom: the maximal mean squared displacement equals to 0.126(1) Å. The strong interionic interaction between the NH fragment of triethylammonium and the B9(H)-B10(H)-B12(H) face of borane cage is of particular interest. This non-covalent bonding pattern was found to be more symmetric than similar CH…H_3B_3 interaction discussed above: the N1C-H1NC-B angles, the H1NC…B and H1NC…H(B) distances vary in narrow ranges (154.1 – 159.0°, 2.495 – 2.603 Å and 2.151 – 2.361 Å, respectively) and the angle formed by the N1C and H1NC atoms and the centroid of the B9-B10-B12 face equals to 176.9°. The analysis of Cambridge Structural Database (CSD)[10] together with additional DFT calculations were also performed to elaborate more on this specific interaction which can be considered as the combination of three N-H…H-B dihydrogen bonds.[11]

According to the CSD processing based on crystal structures with normalized X-H bond lengths, the N-H…H_3B_3 contacts with all three formally non-bonded H…B distances being smaller than the corresponding sum of van der Waals radii appear in 173 structures (from 1029 hits containing B_3H_3 and NH fragments). Despite such contacts are mainly formed between counter-ions, several structures with the N-H…H_3B_3 interactions between substituted borate anions are also known. The distribution of geometrical characteristics suggests that this contact is rather flexible: the triples of H…B distances are characterized by large unbiased variances (up to 0.2 $Å^2$) while their mean varies in a very wide range from 2.42 to 3.13 Å. Nevertheless, the distribution of N-H-centroid angles is significantly skewed towards high values (225 fragments with the angle larger than 150° from 318 – the total number of fragments) that agrees well with the symmetric character of this interaction observed in crystallosolvate of salt [**11**].

A pronounced strength and clear structural preferences of the N-H…H_3B_3 interaction also follows from the DFT geometry optimization of corresponding ionic pair captured from the

crystal structure of [**11**]×acetone. As expected, the geometry features of the N-H…H_3B_3 interaction becomes even more symmetric for the optimized structure which does not suffer from other crystal packing effects: the H…B distances are nearly the same (2.271-2.310 Å) and the N-H-centroid angle equals to 179.0°. The root mean-square deviation for the best overlap between non-hydrogen atoms of crystal and gas geometries is only 0.20 Å even without modelling of non-specific solvation effects. The QTAIM analysis[12] of theoretical electron density function ρ(r) revealed a number of (3,-1) critical points corresponding to diatomic bonding interactions[13] between counter-ions (nine H…H interactions between CH and BH groups and the only one desirable H1NC…B12 interaction, see Figure S1 in Supporting Information). Although all of these interactions are of closed-shell type, their cumulative strength estimated by means of the surface integrals scheme[14] exceeds 15.6 kcal·mol^{-1}. It is to be especially noted that the contribution from the H1NC…B12 interaction plays the role of leading motif in this bonding pattern: its estimated energy equals to 3.4 kcal·mol^{-1} while each H…H interaction contributes only *ca.* 1.4 kcal·mol^{-1} (in average).

Despite strength and structural preferences of the N-H…H_3B_3 interaction, it is of significantly non-directional character as revealed by the reduced density gradient map[15] (see Figure S4) and the value of ρ(r) ellipticity[16] at the H1NC…B12 critical point (>0.59). Supporting formal consideration of the N-H…H_3B_3 interaction as the result of competition between three N-H…H-B dihydrogen bonds, its non-directionality also follows from the analysis of source function of ρ(r)[17]: the main sources of ρ(r) value at the H1NC…B12 critical point raise from the N1C atom and hydrogen atoms of B9(H)-B10(H)-B12(H) face (from 0.002 up to 0.005 a.u.) while the H1NC and corresponding boron atoms play the role of main sinks of electron density (from -0.003 up to -0.009 a.u.).

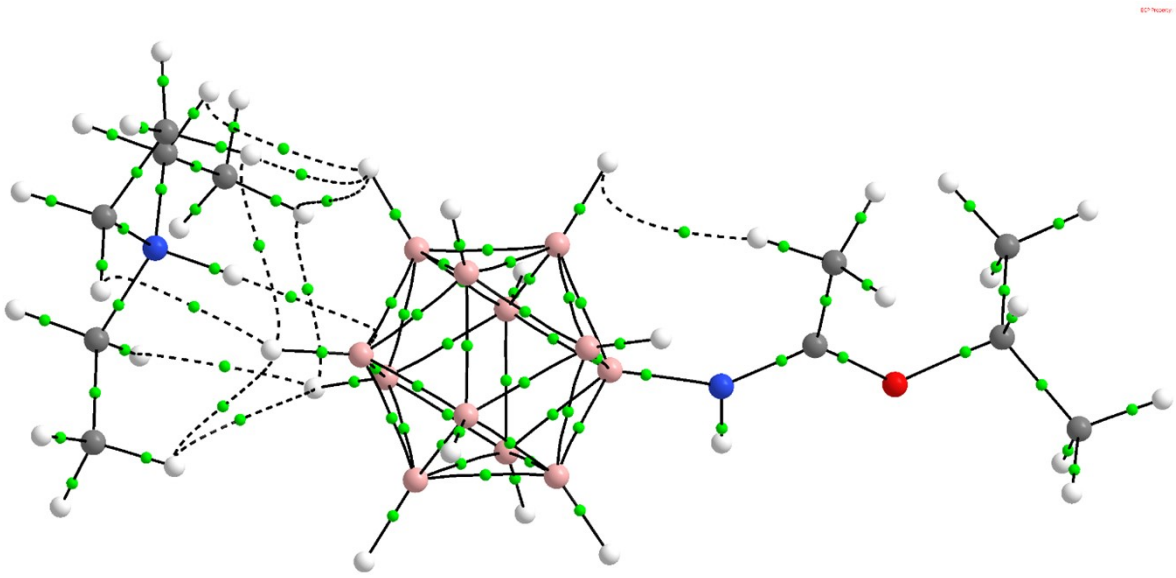

Figure S3. Atomic connectivity graph for the optimized geometry of ionic pair from [**11**]. Small green spheres denote positions of (3,-1) critical point of electron density ρ(r) whereas dashed curves correspond to so-called bond paths for diatomic interactions of closed-shell type (values of $\nabla^2\rho(r)$ and electronic energy density at (3,-1) critical points of ρ(r) are positive).

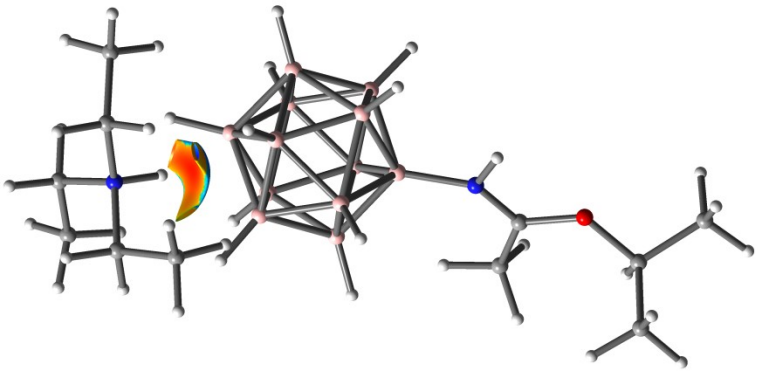

Figure S4. The sign(λ_2)·ρ(r) function (λ_2 is intermediate eigenvalue of ρ(r) Hessian) mapped on the isosurface of reduced density gradient in the area of N-H…H_3B_3 interaction in the ionic pair from [**11**]. Negative, zero and positive values are colored by, respectively, red, green and blue.

Crystal structure of [14]$H_2N(CH_2CH_2)_2O$

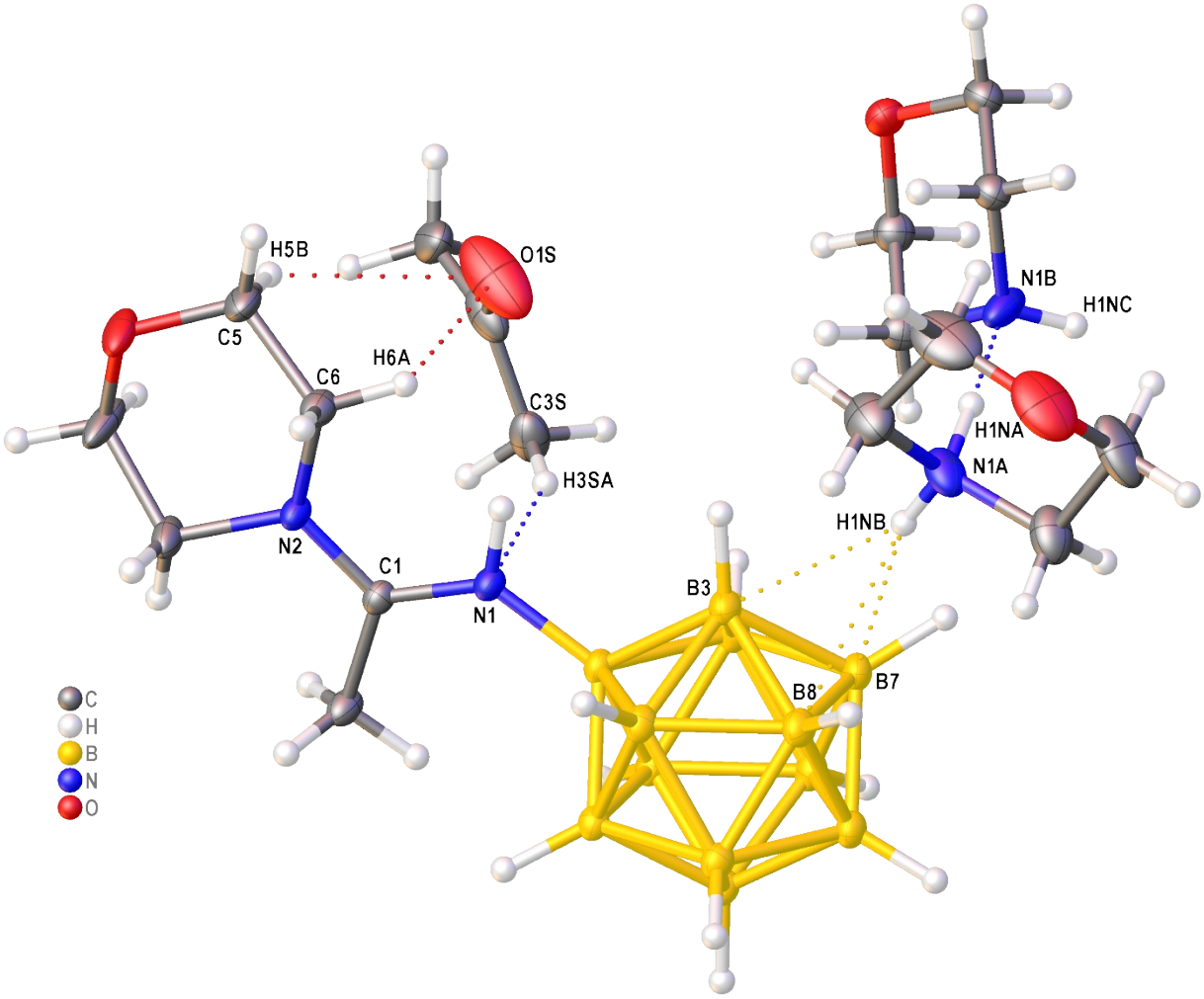

Figure S5. The independent unit of [**14**]×acetone crystal with the representation of non-hydrogen atoms by probability ellipsoids of atomic displacements (p=0.5). Dotted lines correspond to selected non-covalent interactions discussed in the main text. Disordered part of the cation is omitted for clarity.

As in [**11**]×acetone, there is a solvate acetone molecule in crystals of [**14**] which is bounded mainly to the anionic fragment by weak C-H…O and C-H…N interactions (with normalized C-H bond lengths the H…X distances vary in the range of 2.59-2.70 Å).The structure of anion in crystal of [**14**] is in general similar to that of [**11**] and other substituted dodecaborates. However, the C1-N1 bond length in [**14**] is slightly elongated as compared to [**11**] (1.318(1) Å). This can be rationalized by the π-delocalization within the N1-C1-N2 fragment: the C1-N2 bond length is nearly the same and equals 1.340(1) Å. Noteworthy, the delocalization increases upon the transition of anion structure from isolated to condensed state: the DFT optimization in gas yields structure with significantly alternating C1-N1 and C1-N2 bonds (1.292 and 1.370 Å,

respectively) whereas the calculation accounting for non-specific solvation effects (SCRF-PCM model, ε=72) perfectly reproduces the experimental values (1.311 and 1.342 Å). The solvation also affects the charge distribution in the anion. In the gas phase, the NBO atomic charges of the N1 and N2 atoms are respectively -0.63e and -0.50e. The treatment of solvation effects gives -0.71 for the N1 atom and -0.46 for the N2 atom. Thus, the charge of N2 atom of morpholine substituent becomes effectively more positive in the condensed state while the N1 atom, on contrary, gather more electrons. This is in line with the ^{11}B-NMR spectral data obtained for [**14**] in solution.

The cationic fragment in the acetone crystallosolvate of morpholinium salt [**14**] can be considered as the rare case of solvated proton bound between two morpholine species by a strong NH…N hydrogen bond (the N1A…N1B distance is 2.722 Å, the N1A-H1NA-N1B angle equals to 173.9° with the N1A-H1NA being normalized). The strong character of this H-bond is confirmed by the analysis of H1NA atom parameters obtained from the free refinement: the N1A-H1NA distance is 1.059 Å and the isotropic displacement parameter equals to 0.067 Å^2. These values can indicate either the disorder of the H1NA atom along the H-bond line or its movement within a rather flat potential that is common for strong hydrogen bonds.[18] We note, that despite the disorder of the formally neutral morpholine fragment over two places (1:1 ratio), all attempts to localize and refine possible second position of the H1NA atom were unsuccessful. The DFT calculations were conducted to understand factors governing the proton position. Both optimized structures of isolated cationic fragment corresponding to two possible H1NA positions closely reproduce experimental geometry in the area of H-bond: the N1A…N1B distance are 2.694 and 2.695 Å, the N1A-H1NA-N1B angle equal to 175.1° and 175.6°, the N1A-H1NA distances are 1.122 and 1.572 Å, the N1B-H1NA distances are 1.575 and 1.124 Å. We note that the mutual orientation of morpholine species observed in crystal is preserved in these isolated structures: the root mean-square difference for the best overlap of non-hydrogen atoms of crystal and gas geometries was smaller than 0.1 Å in both cases. The sound structural similarity of calculated minimums is in line with the negligibly small difference of their total electronic energies (less than 0.15 kcal·mol^{-1}). Together with the small energy barrier of proton transfer (only 0.7 kcal·mol^{-1} as revealed by the scan of potential energy surface along the coordinate of N1A-H1NA bond stretching), it indicates that the media effects play the main role in stabilization of the N1A-H1NA…N1B bonding regime in crystal.

In contrast to [**11**]×acetone, the main motif of crystal packing of [**14**]×acetone is infinite chains (Figure S6): alternating cationic and anionic fragments are bound into chains by the familiar symmetric N-H…H_3B_3 interactions. Both ‘free’ N-H groups of the cationic moiety are involved

in these interactions with two neighboring anions: the N1B-H1NC fragment is in contact with the B5(H)-B6(H)-B10(H) face and the N1A-H1NB fragment form contacts with the B3(H)-B7(H)-B8(H) face. Geometry criteria suggest that the second interaction is stronger: H1NC…B distances vary from 2.662 to 2.674 Å while H1NB…B distances do in a range of 2.418-2.532 Å; the N1B-H1NC-centroid and N1A-H1NB-centroid angles are 167.9° and 177.5°, respectively (N-H bond lengths were normalized). This is in concordance with the surface integral estimations[14] of energies of diatomic bonding interactions retrieved within the QTAIM formalism between counterions of the isolated associate containing one cationic and two neighboring anionic fragments (only the H1NA atom position were optimized while other X-H bond lengths were normalized, see bottom scheme on Figure 4). The net energy of non-covalent bonding between ions bounded by the N1A-H1NB…H_3B_3 interaction equals to 6.8 kcal·mol^{-1} while the energy of other cation-anion interaction is only 5.6 kcal·mol^{-1}. Again, as in [**11**]×acetone, the (N)H…B diatomic interactions play the key role: the H1NB…B interaction is more favorable than the H1NA…B one (2.5 and 1.5 kcal·mol^{-1}, respectively). The difference in strength of non-covalent bonding between counterions agrees well with the distribution of formal atomic charges: the morpholine moiety having quaternized N1A atom forms stronger interionic interactions. Vice versa, the corresponding transfer of negative charge due to stronger interionic interactions is compensated by the stabilization of the N1A-H1NB…N1B bonding regime[19]. Indeed, the optimization of second H1NA atom position in the associate produces structure which is less favorable (on 2.3 kcal·mol^{-1}).

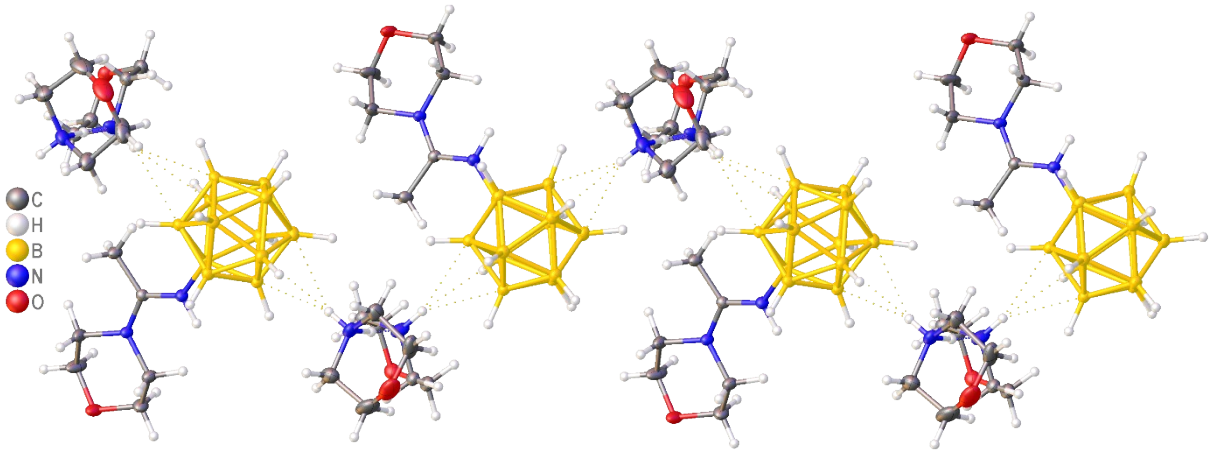

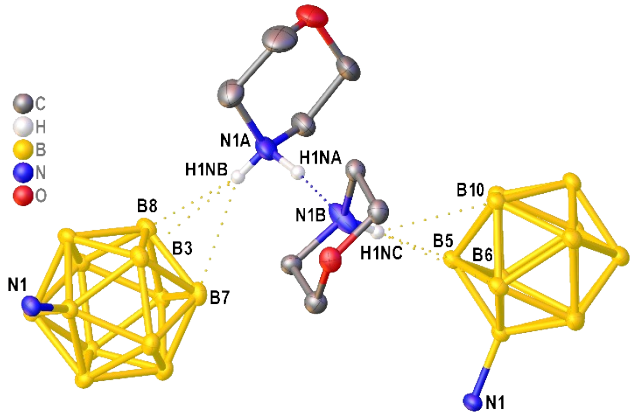

Figure S6. A fragment of infinite chain (top) and the schematic view of the N-H…H_3B_3 interionic interactions (bottom, substituents of the borane cages and most of hydrogen atoms are omitted for clarity) in the [**14**]×acetone crystal.

---

1. Gaussian 09, Revision D.01, M. J. Frisch, G. W. Trucks, H. B. Schlegel, G. E. Scuseria, M. A. Robb, J. R. Cheeseman, G. Scalmani, V. Barone, G. A. Petersson, H. Nakatsuji, X. Li, M. Caricato, A. Marenich, J. Bloino, B. G. Janesko, R. Gomperts, B. Mennucci, H. P. Hratchian, J. V. Ortiz, A. F. Izmaylov, J. L. Sonnenberg, D. Williams-Young, F. Ding, F. Lipparini, F. Egidi, J. Goings, B. Peng, A. Petrone, T. Henderson, D. Ranasinghe, V. G. Zakrzewski, J. Gao, N. Rega, G. Zheng, W. Liang, M. Hada, M. Ehara, K. Toyota, R. Fukuda, J. Hasegawa, M. Ishida, T. Nakajima, Y. Honda, O. Kitao, H. Nakai, T. Vreven, K. Throssell, J. A. Montgomery, Jr., J. E. Peralta, F. Ogliaro, M. Bearpark, J. J. Heyd, E. Brothers, K. N. Kudin, V. N. Staroverov, T. Keith, R. Kobayashi, J. Normand, K. Raghavachari, A. Rendell, J. C. Burant, S. S. Iyengar, J. Tomasi, M. Cossi, J. M. Millam, M. Klene, C. Adamo, R. Cammi, J. W. Ochterski, R. L. Martin, K. Morokuma, O. Farkas, J. B. Foresman, and D. J. Fox, Gaussian, Inc., Wallingford CT, 2016.

2. J. Perdew, M. Ernzerhof, K. Burke, *J.Chem. Phys.*, 1996, *105*, 9982.

3. A. Carlo, V. Barone, J. Chem. Phys., 110, 1999, 6158

4. S. Grimme, S. Ehrlich and L. Goerigk, “Effect of the damping function in dispersion corrected density functional theory,” J. Comp. Chem. 32 (2011) 1456-65

5. T. Lu, F. Chen, J. Comput. Chem. 2012, 33, 580-592.

6. AIMAll (Version 19.02.13), T. Keith, TK Gristmill Software, Overland Park KS, USA, 2016 (aim.tkgristmill.com).

7. Reed A. E.; Curtiss L. A.; Weinhold F. Intermolecular interactions from a natural bond orbital, donor-acceptor viewpoint. Chem. Rev. 1988, 88, 899-926.

8. S.Hoffmann, E.Justus, M.Ratajski, E.Lork, D.Gabel, J. Organomet. Chem., 2005, 690, 2757
9. Reed A. E.; Curtiss L. A.; Weinhold F. Intermolecular interactions from a natural bond orbital, donor-acceptor viewpoint. Chem. Rev. 1988, 88, 899
10. The Cambridge Structural Database. C. R. Groom, I. J. Bruno, M. P. Lightfoot and S. C. Ward, Acta Cryst. (2016). B72, 171
11. Natalia V. Belkova, Elena S. Shubina, and Lina M. Epstein "Diverse World of Unconventional Hydrogen Bonds" *Acc. Chem. Res.*, 2005, 38, 624
12. The Quantum Theory of Atoms in Molecules: From Solid State to DNA and Drug Design", Edited by C.F. Matta and R.J. Boyd, WILEY-VCH, Weinham, (2007)
13. A. M. Pendas, E. Francisco, M. A. Blanco, C. Gatti, Chem. Eur. J. 2007, 13, 9362-9371; A. A. Anisimov, I. V. Ananyev, J. Comput. Chem., 2020, 41, 2213
14. A. A. Romanova, K. A. Lyssenko, I. V. Ananyev, J. Comput. Chem. 2018, 39, 1607
15. E. R. Johnson, S. Keinan, P. Mori-Sánchez, J. Contreras-García, A. J. Cohen, W. Yang, *J. Am. Chem. Soc.* **2010**, *132*, 18, 6498
16. I. V. Ananyev, K. A. Lyssenko, *Mendeleev Commun.* **2016**, *26*, 338
17. C. Gatti, F. Cargnoni, L. Bertini, J. Comput. Chem., 2003, 24, 422.
18. I.V. Ananyev, I.S. Bushmarinov, I.E. Ushakov, A.I. Aitkulova, K.A. Lyssenko, RSC Adv, 2015, 5, 97495
19. Ananyev, I.S. Bushmarinov, I.E. Ushakov, A.I. Aitkulova, K.A. Lyssenko, RSC Adv, 2015, 5, 97495-97502